Optical second-harmonic generation in thin film systems

Optical second-harmonic generation in thin film systems

J. J. H. Gielis, P. M. Gevers, I. M. P. Aarts,
M. C. M. van de Sanden, and W. M. M. Kessels[a)]
Department of Applied Physics, Eindhoven University of Technology, P.O. Box 513, 5600 MB Eindhoven, The Netherlands

(Received 19 May 2008; accepted 2 September 2008; published 3 November 2008)

The surface and interface sensitive nonlinear optical technique of second-harmonic generation (SHG) is a very useful diagnostic in studying surface and interface properties in thin film systems and can provide relevant information during thin film processing. An important aspect when applying SHG is the interpretation of the SHG response. In order to utilize the full potential of SHG during materials processing it is necessary to have a good understanding of both the macroscopic and the microscopic origin of the SHG response, particularly in thin film or multilayer systems where the propagation of radiation is another important aspect that should be considered carefully. A brief theoretical overview on the origin of the SHG response and a description of the propagation of radiation will be given. Furthermore, several methods will be discussed that might reveal the possible macroscopic and microscopic origins of the SHG response in thin film systems. The different approaches will be illustrated by examples of real-time and spectroscopic SHG experiments with thin film systems relevant in Si etching and deposition environments, such as (1) hydrogenated amorphous Si films deposited by hot-wire chemical vapor deposition on both Si(100) and fused silica substrates, (2) amorphous Si generated by low-energy Ar^+-ion bombardment of H terminated Si(100), and (3) Al_2O_3 films deposited by plasma-assisted atomic layer deposition on H terminated Si(100). © *2008 American Vacuum Society.* [DOI: 10.1116/1.2990854]

I. INTRODUCTION

The nonlinear optical technique of second-harmonic generation (SHG) is an established technique in surface science, particularly in studies on crystalline silicon (*c*-Si).[1–8] Crucial for the success of SHG is the sensitivity of the technique to surfaces and buried interfaces and the ability to resolve optical transitions. The sensitivity of SHG to surfaces and interfaces arises from the fact that, within the electric dipole approximation, SHG is forbidden in the bulk of centrosymmetric media such as *c*-Si and amorphous thin films. Microscopically, SHG is the conversion of two photons with energy $\hbar\omega$ into a single photon with energy $2\hbar\omega$. When the photon energy of either the fundamental or the SHG radiation is close to an optical transition in the medium, the SHG response is resonantly enhanced. Furthermore, being an all-optical technique, SHG is noninvasive and contactless, can be applied *in situ*, and has real-time applicability with a good time resolution. These characteristics make SHG also a very promising diagnostic in materials processing, particularly in thin film processing related to Si technology. As surface and interface properties increasingly govern future device performance, SHG can be very beneficial in device optimization by providing real-time process feedback and control. The technique can also provide more understanding of fundamental mechanisms that govern surface and interface related processes and can yield more insight into resulting material properties.

In general, a very important issue in the application of SHG is the interpretation of the SHG response. Aspects such as the macroscopic origin (i.e., the geometrical origin) and the microscopic origin (i.e., the source of SHG on an atomic level) of the SHG response need to be considered carefully. When applying SHG during processing of thin films the propagation of radiation through the thin film system is an additional issue that has to be taken into account. In this article, the application of SHG during processing of thin film systems related to Si technology will be explored. Several approaches to reveal the origin of the SHG response will be discussed and illustrated with examples including SHG measurements with (1) hydrogenated amorphous Si (*a*-Si:H), (2) amorphous Si (*a*-Si), and (3) Al_2O_3 thin films, predominantly on *c*-Si substrates.

In the interpretation of SHG data from thin film systems related to Si technology, an important starting point is information reported in *c*-Si surface science, where SHG has been applied extensively to study clean and H terminated *c*-Si surfaces. For example, from controlled H dosing experiments of clean *c*-Si surfaces, SHG has been shown to be sensitive to surface Si dangling bonds in the fundamental photon energy range of ~1.0–~1.3 eV.[2,3,6] These surface dangling bonds form states in the band gap of *c*-Si. Furthermore, two-photon resonances close to 3.4 eV have been observed at *c*-Si surfaces. These resonances have a similar appearance as resonances observed with linear optical techniques, such as spectroscopic ellipsometry, around 3.4 eV that are related to the E_0'/E_1 critical point (CP) transitions of bulk *c*-Si.[9] From this similarity, it was concluded that the SHG response was also related to E_0'/E_1 CP transitions.[1] More specifically, these resonances were suggested to originate from Si–Si bonds distorted or strained due to the presence of a surface or

a)Electronic mail: w.m.m.kessels@tue.nl

interface.[1] In addition, the presence of dc electric fields leading to electric-field-induced second-harmonic (EFISH) generation was shown to influence these resonances.[4] The technologically very relevant SiO_2/c-Si interface has also been investigated thoroughly with SHG, as reviewed by Lüpke.[10] For this system the same resonances were observed around the c-Si E_0'/E_1 CP energy of 3.4 eV, originating from distorted Si–Si bonds and EFISH from the c-Si space-charge region. At higher SHG photon energies, resonances were observed around 4.3 eV, near the c-Si E_2 CP, and around 3.7 eV. The latter resonance was attributed to interband transitions in Si in a thin transition layer between Si and SiO_2.[5,7,8] In addition, the SiO_2/c-Si system was the first system where time-dependent variations in the SHG intensity due to photon-induced charge trapping, which resulted in changes in the EFISH contribution, were observed.[10–13]

The characterization of (hydrogenated) amorphous Si films by SHG as used in this study is relatively unexplored. Erley and Daum[5] reported on *ex situ* SHG experiments of a 0.7 μm thick a-Si:D film on Si(100) and observed a very weak featureless SHG spectrum that was an order of magnitude lower in intensity than for native oxide covered Si(100). Alexandrova *et al.*[14] performed *ex situ* SHG experiments on a-Si:H films deposited on different glass substrates but only at a fixed photon energy of 1.17 eV (1064 nm) using a neodymium doped yttrium aluminum garnet (Nd:YAG) laser. We reported on both *ex situ* and real-time *in situ* SHG experiments of a-Si:H deposited on fused silica substrates investigated using a Nd:YAG-pumped optical parametric oscillator (OPO) that allowed for spectroscopic measurements. In these studies broad spectral features assigned to both dangling bonds and Si–Si bonds were observed.[15,16] In this article examples of real-time and spectroscopic SHG experiments with (hydrogenated) amorphous Si films on c-Si substrates using femtosecond Ti:sapphire lasers will be addressed.[17–21]

Recently, SHG has also been applied in the field of high-κ dielectrics. Because of its sensitivity to internal electric fields, SHG (or to be more precise EFISH) is very suitable in characterizing the charge present in thin films of high-κ dielectrics on c-Si. Studies include time-dependent photon-induced charge trapping and process-dependent charging in stacks of c-Si and the high-κ dielectrics Al_2O_3, HfO_2, ZrO_2, $ZrSi_xO_y$, and $HfSi_xO_y$.[22–25] These studies mainly focused on the application of the high-κ materials to replace SiO_2 as a gate dielectric in metal-oxide-semiconductor structures, where the presence of a fixed charge adversely affects device performance. However, Al_2O_3 has also been shown to provide an excellent level of surface passivation of c-Si, which is vital for the performance of devices such as light emitting diodes, photodetectors, and high-efficiency solar cells.[26–28] For this application the presence of a fixed charge appears to be beneficial. It will be discussed that spectroscopic SHG is very suitable in characterizing process-dependent fixed charges in Al_2O_3.

Although not as extensively as in c-Si surface science, SHG has been applied in a few other studies that are related to Si-based materials processing. For example, epitaxial growth of Si thin films has been studied during dissociative chemisorption of Si_2H_6 on clean Si surfaces at high temperatures (>750 K). In these experiments it was found that the SHG response was predominantly governed by variations in H coverage.[4,29] Heinz *et al.*[30] performed SHG experiments during ion bombardment of c-Si. They observed decreasing anisotropic SHG contributions in Si(111)-7×7 during bombardment with 5 keV Ar^+ ions at a fixed SHG photon energy of 2.33 eV.

In this article, an overview is given of aspects that arise when applying SHG in thin film systems. First, a summary is given of the theory that describes SHG and that forms a basis for the interpretation of the SHG data. Furthermore, the macroscopic origin of SHG is presented in more detail and the possible influence of bulk contributions is discussed. Then, the microscopic origin of SHG and the propagation of radiation in thin film geometries are addressed. After this theoretical section, the laser systems and the optical setups used to perform SHG experiments as well as sample preparation methods, as used in this study, will be addressed. Subsequently, examples of SHG measurements in thin film systems related to Si technology are presented focusing on the separation of surface, interface, and possible bulk contributions. The results include the SHG response of the substrates, the SHG response of thin films without the influence of substrates, and the SHG response for thin film–substrate systems with possible substrate contributions.

II. REVIEW OF SHG THEORY

A. Macroscopic origin

1. Dipolar SHG

Optical radiation with electric field $\mathbf{E}$ interacts with a medium by inducing a polarization $\mathbf{P}$ in this medium, as given by

$$\mathbf{P} = \varepsilon_0 \vec{\vec{\chi}} \cdot \mathbf{E}, \tag{1}$$

where ε_0 is the vacuum permittivity and $\vec{\vec{\chi}}$ is the electric susceptibility, which is a second-rank tensor describing the response of the medium. Generally, the induced polarization has the same frequency as the incident electric field and describes linear optical phenomena such as refraction and reflection. However, for high intensity optical radiation involving strong electric fields, higher order contributions start to play a role. Within the electric dipole approximation, i.e., assuming spatially homogeneous fields, the induced polarization can be represented as an expansion of the electric field,[31]

$$\mathbf{P} = \varepsilon_0 \vec{\vec{\chi}}^{(1)} \cdot \mathbf{E} + \varepsilon_0 \vec{\vec{\chi}}^{(2)} : \mathbf{EE} + \varepsilon_0 \vec{\vec{\chi}}^{(3)} : \mathbf{EEE} + \cdots, \tag{2}$$

where $\vec{\vec{\chi}}^{(n)}$ is the nth order susceptibility, which is a tensor of rank $n+1$. An important consequence of Eq. (2) is that also components at other frequencies than the fundamental frequency of the incident radiation contribute to the polarization, as can be recognized by explicitly including the frequency of the electric fields, $\mathbf{E}(\omega) = \mathbf{E}e^{i\omega t}$. The nonlinear

optical effect of second-harmonic generation is described by the second term at the right hand side of Eq. (2),

$$\mathbf{P}^{(2)}(2\omega) = \varepsilon_0 \vec{\chi}^{(2)}(2\omega):\mathbf{E}(\omega)\mathbf{E}(\omega). \tag{3}$$

This equation shows the production of radiation at twice the incident frequency. When two different input frequencies are applied, a more general nonlinear optical effect occurs, sum-frequency generation, where the output frequency is a linear combination of both incident frequencies. The second-order nonlinear susceptibility tensor $\vec{\chi}^{(2)}$ is a tensor with 27 components $\chi^{(2)}_{ijk}$ that relate the second-order polarization component i to the components j and k of the incident electric fields, where $i,j,k \in \{x,y,z\}$. For SHG it is irrelevant in which order the incident electric field components appear; consequently the second-order susceptibility tensor is symmetric in the last two indices: $\chi^{(2)}_{ijk}=\chi^{(2)}_{ikj}$. Due to this permutation symmetry, $\vec{\chi}^{(2)}$ reduces to 18 independent components. The actual independent and nonzero components $\chi^{(2)}_{ijk}$ depend on the medium the tensor $\vec{\chi}^{(2)}$ describes. An important case is that of centrosymmetric materials, which are materials with centers of inversion symmetry being invariant under the transformation $\mathbf{r} \rightarrow -\mathbf{r}$. Since $\vec{\chi}^{(2)}$ is a material property, it has the same symmetry properties as the material itself. As a result, for centrosymmetric media every component $\chi^{(2)}_{ijk}$ is necessarily equal to its inverted counterpart, $\chi^{(2)}_{ijk}=-\chi^{(2)}_{ijk}$. Obviously, this relation only holds for $\chi^{(2)}_{ijk}=0$. Consequently, no SHG will occur in the bulk of these centrosymmetric media. Centrosymmetry is a macroscopic property, i.e., a medium and its image are compared under inversion averaged over a macroscopic volume with maximum length scales on the order of the wavelength of the applied radiation. Hence, centrosymmetric materials include both crystalline materials, such as Si, and amorphous materials, such as amorphous silicon and amorphous oxides.

The discussion so far only applies to bulk properties. At surfaces and interfaces, however, the inversion symmetry is broken and not all components $\chi^{(2)}_{ijk}$ reduce to zero. In this work we mainly focus on surfaces and interfaces of Si(100) and amorphous films such as *a*-Si:H, *a*-Si, and Al_2O_3. The surfaces and interfaces of these materials are part of symmetry classes $4mm$ and ∞m, respectively.[32] For these symmetry classes only five components of the second-order nonlinear susceptibility tensor are nonzero, of which only three components are independent. The nonzero components are $\chi^{(2)}_{zzz}$, $\chi^{(2)}_{zxx}=\chi^{(2)}_{zyy}$, and $\chi^{(2)}_{xxz}=\chi^{(2)}_{yyz}$,[15,32] where x and y define the surface or interface plane with z orthogonal to this plane. In addition, x and z lie within the plane of incidence and y is orthogonal to it, as shown in Fig. 1. The surface SHG response described by these components is isotropic. Depending on the selected polarization of the fundamental and SHG radiation, different tensor components contribute to the surface and interface SHG responses, resulting in (local) maxima in the SHG signal for three different combinations: (1) p polarized fundamental and p polarized SHG radiation (pP polarization), where all three independent tensor components contribute, (2) s polarized fundamental and p polarized SHG radiation (sP polarization), where only $\chi^{(2)}_{zxx}$ contributes,

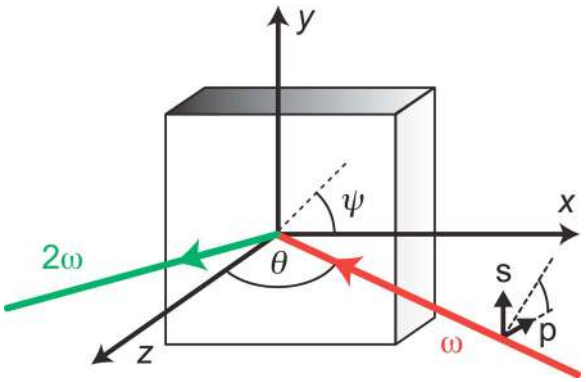

FIG. 1. Definition of the coordinate axes and the polarization geometry. Radiation with the electric field parallel (perpendicular) to the plane of incidence is referred to as $p(s)$ polarized. The angles θ, φ, and ψ denote the angle of incidence, the polarization angle of the fundamental radiation, and the azimuthal angle, respectively.

and (3) mixed fundamental polarization with equal s and p components and s polarized SHG radiation (mix$S$ polarization), where only $\chi^{(2)}_{xxz}$ contributes. This polarization dependence satisfies the following expression for the p and s polarized SHG intensities, $I_p(2\omega)$ and $I_s(2\omega)$:[16,32]

$$I_p(2\omega) = a\,\sin^4(\varphi) + b\,\sin^2(\varphi)\cos^2(\varphi) + c\,\cos^4(\varphi),$$

$$I_s(2\omega) = d\,\sin^2(\varphi)\cos^2(\varphi), \tag{4}$$

where the coefficients $a-d$ depend on the different tensor components and the linear optical propagation of radiation. The angle φ denotes the angle between the polarization vector of the fundamental radiation and the plane of incidence (see Fig. 1).

2. Electric-field-induced SHG

Apart from the electric dipole term given by Eq. (3), radiation at the second-harmonic photon energy can also result from other sources. One of these processes is EFISH, which is a third-order process where one of the driving fields is a dc field.[33] Such dc electric fields can be present in the space-charge region at semiconductor surfaces arising when surface states pin the surface Fermi energy close to the midgap, resulting in band bending.[34] Also a fixed charge in the system or the application of an external dc bias can result in dc electric fields and generate EFISH.[11,12,33] Both the internal and the applied dc electric fields penetrate to a distance below the surface determined by the bulk doping concentration.[34,35] This effect exhibits essentially bulk spectroscopic properties and is referred to as bulk EFISH. Strong dc electric fields can also be present in the top two to three atomic monolayers, e.g., in the reconstructed Si(100) surface where valence electrons are redistributed into buckled dimers.[4,34] This effect is referred to as surface EFISH. With both bulk and surface contributions, the nonlinear polarization responsible for generating SHG radiation can be written as[34]

$$\mathbf{P}(2\omega) = \varepsilon_0 \overleftrightarrow{\chi}^{(2)}(2\omega):\mathbf{E}(\omega)\mathbf{E}(\omega) + \varepsilon_0 \overleftrightarrow{\chi}_S^{(3)}(2\omega):\mathbf{E}(\omega)\mathbf{E}(\omega)\mathbf{E}_{\mathrm{dc}}^{\mathrm{surf}} + \varepsilon_0 \overleftrightarrow{\chi}_B^{(3)}(2\omega):\mathbf{E}(\omega)\mathbf{E}(\omega)\mathbf{E}_{\mathrm{dc}}^{\mathrm{bulk}}, \quad (5)$$

where the first term denotes the dipole contribution from Eq. (3), the second term the surface EFISH contribution, and the third term the bulk EFISH contribution. The susceptibility tensors describing the third-order effect of EFISH are tensors of rank 4. However, with a dc electric field in the z direction, i.e., perpendicular to the surface, the symmetry properties of the EFISH terms are identical to the "regular" surface dipole contribution. Bulk EFISH contributes significantly to SHG for sufficiently high dc electric fields, typically $E_{\mathrm{dc}}^{\mathrm{bulk}} > 10^5$ V cm^{-1}.[11,33] In dc-biased metal-oxide-semiconductor structures, such dc fields can be reached for external bias voltages on the order of volts.[33] For an unbiased semiconductor a significant dc electric field can be caused by the doping density.[4] For the n-type Si(100) substrates applied in this work the doping density is low, around 2.5×10^{14} cm^{-3}, and the electric field at the surface can be estimated to be <4 kV cm^{-1}.[36,37] Consequently, the influence of EFISH from the Si space region is negligible for these substrates.

The effect of EFISH can also arise or change because of SHG experiments. The incident high intensity radiation can locally cause photon-induced charge trapping and thereby modify the internal electric fields. Significant photon-induced charge trapping results in a time-dependent change in SHG response. Both for SiO_2 and high-κ dielectrics on c-Si, the trapping process has been reported to occur via injection of electrons from the c-Si valence band into the oxide conduction band. The injected charge then diffuses into trap sites in the oxide bulk, at the buried interface, or at the ambient surface.[12,23–25]

3. Bulk SHG

In addition to dipolar SHG and EFISH, another source of SHG radiation can occur: SHG from multipole contributions. The contributions discussed so far resulted from the electric dipole approximation. In this approximation the electric fields are assumed to be spatially homogeneous; consequently the induced polarization is a function of the electric field at position $\mathbf{r}$. In order to extend the description beyond this approximation, the induced polarization has to be expanded in a nonlocal way by taking into account the electric field distribution in the vicinity of $\mathbf{r}$. This approach reveals the presence of multipole contributions. These multipole contributions are an important issue in the application of SHG as a pure surface or interface probe since these contributions can cause bulk SHG in situations where dipolar bulk SHG is forbidden. The leading-order multipole contributions, in addition to the electric dipole contribution, are the electric quadrupole and magnetic dipole contributions, as shown by[32,38,39]

$$\mathbf{P}(2\omega) = \varepsilon_0 \overleftrightarrow{\chi}^{(2)}(2\omega):\mathbf{E}(\omega)\mathbf{E}(\omega) + \varepsilon_0 \overleftrightarrow{\chi}_Q^{(2)}(2\omega):\mathbf{E}(\omega)\,\nabla\,\mathbf{E}(\omega) + \cdots. \quad (6)$$

The first term in Eq. (6) is again the dipole contribution presented in Eq. (3). The second term includes the electric quadrupole and magnetic dipole contributions. The nonlocal character is reflected by the gradient operator in this term, where $\overleftrightarrow{\chi}_Q^{(2)}$ is the second-order quadrupolar susceptibility that is a tensor of rank 4 with 81 components. Again, the actual independent and nonzero components depend on the medium described by $\overleftrightarrow{\chi}_Q^{(2)}$. For the bulk of centrosymmetric media the electric dipolar susceptibility $\overleftrightarrow{\chi}^{(2)}$ vanishes and the second term of Eq. (6) governs the nonlinear polarization. For a cubic centrosymmetric material the only independent nonvanishing elements of $\overleftrightarrow{\chi}_Q^{(2)}$ are $\chi_{Q,iiii}^{(2)}$, $\chi_{Q,iijj}^{(2)}$, $\chi_{Q,ijij}^{(2)}$, and $\chi_{Q,ijji}^{(2)}$, with $i \neq j$. These components are usually represented by the phenomenological parameters β, γ, δ, and ζ, which consist of a linear combination of the four independent tensor components.[38–41] The nonlinear polarization can now be written in components as

$$\mathbf{P}_{Qi}(2\omega) = \varepsilon_0(\delta - \beta - 2\gamma)(\mathbf{E}\cdot\nabla)E_i + \varepsilon_0\beta E_i(\nabla\cdot\mathbf{E}) + \varepsilon_0\gamma\nabla_i(\mathbf{E}\cdot\mathbf{E}) + \varepsilon_0\zeta E_i\nabla_i E_i. \quad (7)$$

In the remainder of this section the origin of these four terms and their impact will be discussed. The first three terms of Eq. (7) are present in isotropic media, while the last term proportional to ζ only occurs in anisotropic media. Cubic centrosymmetric media such as crystalline Si are anisotropic with respect to crystal orientation. For these materials the anisotropic term contributes for all polarization combinations of the incident and the SHG radiation.[39] Tom *et al.*[42] showed that for Si(111) and Si(100) the magnitude of the anisotropic quadrupole bulk susceptibility is of the same order as the surface dipole susceptibility, as was recently confirmed by An *et al.*[43] who measured the amplitude and absolute phase of the three surface dipole components and the anisotropic bulk component for Si(100). Li *et al.*[44] showed that for oxidized Si(100), interference of the anisotropic bulk contribution and surface dipole contributions can lead to circular dichroism. In this work we will mainly focus on amorphous films on Si(100) substrates. For these systems all surface and interface dipole contributions as well as possible bulk contributions from the amorphous films are isotropic. This implicates that the origin of any anisotropic contribution in the SHG response can be assigned to the Si(100) substrate only. For example, for both p and s polarized fundamental radiation the dependence of the p and s polarized SHG intensities on the azimuthal orientation of Si(100) satisfies[32,42]

$$I_p(2\omega) = (u + v\cos(4\psi))^2, \qquad I_s(2\omega) = w\sin^2(4\psi), \quad (8)$$

where isotropic contributions are represented by u and the anisotropic bulk contribution by v and w. In addition, u, v, and w include linear optical properties. The azimuthal angle ψ is defined as the angle between the plane of incidence and the [011] crystal axis (see Fig. 1).

TABLE I. Overview of the polarization dependence of the surface dipole contributions and the bulk electric quadrupole/magnetic dipole contributions for centrosymmetric media with $4mm$ and ∞m surface symmetries. ζ only contributes for anisotropic media (indicated by A). Terms proportional to $\delta-\beta-2\gamma$ are only nonzero in a multiple beam geometry. Here the polarization dependence for a thin film geometry with multiple reflections is displayed (indicated by TF).

Component		pP	sP	mix$P$	sS	pS	mix$S$
Surface	$\chi^{(2)}_{zzz}$	√		√			
	$\chi^{(2)}_{zxx}$	√	√	√			
	$\chi^{(2)}_{xxz}$	√		√			√
	ζ	A	A	A	A	A	A
Bulk	γ	√	√	√			
	β						
	$\delta-\beta-2\gamma$	TF		TF			TF

The third term in Eq. (7) proportional to γ is the magnetic dipole contribution that radiates in a manner that is indistinguishable from electric dipole surface or interface contributions. The magnetic dipole term always appears in a linear combination with $\chi^{(2)}_{zxx}$, such as $\chi^{(2)}_{zxx}+\varepsilon^{-1}\gamma$.[39–41] Consequently by choosing s polarized SHG radiation, this bulk term does not contribute.

The second term in Eq. (7) that is proportional to β vanishes in a homogeneous medium because of the zero divergence of the electric field.

The first term in Eq. (7) with prefactor $(\delta-\beta-2\gamma)$ disappears when only a single plane wave is present in the medium since $\mathbf{E}\cdot\mathbf{k}=0$. However, for several experimental configurations, the first term of Eq. (7) does contribute. For example, for a tightly focused Gaussian beam, this term is nonzero and scales with $|\mathbf{E}|^2/w_0$, where w_0 is the beam waist of the incident radiation.[45,46] The first term also contributes when multiple beams are present in the medium, for example, in a thin film geometry where due to multiple reflections a second plane wave occurs.[47] The polarization dependence of this term for the thin film geometry can be evaluated by explicitly including the electric fields $\mathbf{E}_m(\mathbf{r})=\mathbf{E}^0_m e^{i\mathbf{k}_m\cdot\mathbf{r}}$, where $m=1$ and $m=2$ represent the waves propagating in the film toward and away from the substrate, respectively,

$$\begin{aligned}\mathbf{P}_Q(2\omega,\mathbf{r}) = i\varepsilon_0(\delta-\beta-2\gamma)\{&\mathbf{E}^0_1\cdot\mathbf{k}_1\mathbf{E}^0_1 e^{2i\mathbf{k}_1\cdot\mathbf{r}}\\ &+\mathbf{E}^0_1\cdot\mathbf{k}_2\mathbf{E}^0_2 e^{i(\mathbf{k}_1+\mathbf{k}_2)\cdot\mathbf{r}}+\mathbf{E}^0_2\cdot\mathbf{k}_1\mathbf{E}^0_1 e^{i(\mathbf{k}_1+\mathbf{k}_2)\cdot\mathbf{r}}\\ &+\mathbf{E}^0_2\cdot\mathbf{k}_2\mathbf{E}^0_2 e^{2i\mathbf{k}_2\cdot\mathbf{r}}\}.\end{aligned} \tag{9}$$

The first and last terms in Eq. (9) vanish since the electric field of the beams is always perpendicular to the propagation direction, or $\mathbf{E}_i\cdot\mathbf{k}_i=0$. The second and third terms only vanish for s polarized input radiation, as in this case the fundamental electric fields are, by definition, perpendicular to the plane of incidence, or $\mathbf{E}_i\cdot\mathbf{k}_j=0$. For fully p polarized input, Eq. (9) results in a p polarized polarization wave, consequently generating only p polarized SHG radiation. s polarized SHG radiation can be generated by using mixed input polarization.

The term proportional to $\delta-\beta-2\gamma$ also contributes to the SHG response in a two-beam SHG geometry.[45,46,48,49] Consider, for example, a configuration with one beam at normal incidence with respect to the sample surface and the other beam at a certain angle. The electric fields of the two beams can be described again with $\mathbf{E}_m(\mathbf{r})=\mathbf{E}^0_m e^{i\mathbf{k}_m\cdot\mathbf{r}}$, where in this case $m=1$ denotes the beam at normal incidence and $m=2$ the angled beam. The polarization in this situation is also given by Eq. (9). Similar as for the thin film geometry, the first and last terms vanish. If both beams are polarized perpendicular to the plane of incidence (s polarization), thus $\mathbf{E}_1\|\mathbf{E}_2\|\hat{y}$, then also the second and third terms vanish as in this case $\mathbf{E}_i\cdot\mathbf{k}_j=0$. When both beams are polarized parallel to the plane of incidence (p polarization), the SHG polarization is parallel to $\mathbf{k}_1+\mathbf{k}_2$ and, consequently, does not radiate, as derived by Sun *et al.*[45,49] However, when $\mathbf{E}_1\perp\mathbf{E}_2$, for example, $\mathbf{E}_1\|\hat{x}$ and $\mathbf{E}_2\|\hat{y}$, then the third term vanishes since $\mathbf{E}_2\cdot\mathbf{k}_1=0$, whereas the second term does contribute and $\mathbf{P}_Q\|\mathbf{E}_2$, i.e., s polarized. The special case of this so-called cross-polarized two-beam second-harmonic generation has been used to study Si nanocrystals embedded in fused silica.[45,46,48,49]

Returning to the amorphous film/Si(100) substrate geometry, the polarization dependence of all surface dipole and bulk electric quadrupole/magnetic dipole terms contributing for this system are summarized in Table I. In brief, for amorphous thin films on Si(100), isotropic surface dipole components originating from surfaces and interfaces can contribute to the SHG response. The substrate bulk can contribute to the SHG response via the anisotropic bulk term ζ and the magnetic dipole term γ. The bulk of the amorphous film can generate SHG via the $\delta-\beta-2\gamma$ term and magnetic dipole term γ.

In order to separate bulk contributions, surface contributions, and buried interface contributions in thin film systems, several approaches can be used. (1) Specific polarization configurations and azimuthal orientations can be selected. However, as evident from Table I this method does not result in a full separation of surface or interface and bulk contributions. (2) Substrates without a SHG response can be used. (3) The film thickness dependence of the SHG response can be used to distinguish between surface, interface, and bulk contributions. (4) The surface properties can be selectively modified, possibly resulting in a change in SHG response.

Finally, (5) spectroscopic information can be used to reveal the origin of the SHG radiation, providing information not only on the microscopic origin but also on the macroscopic origin. In Sec. IV examples of these approaches will be given for different thin film systems.

B. Microscopic origin

Microscopically, SHG is the conversion of two photons with energy $\hbar\omega$ into a single SHG photon with energy $2\hbar\omega$. An expression for $\vec{\chi}^{(2)}$ can be derived quantum mechanically from perturbation theory, resulting in a sum of eight terms of the form[31]

$$\chi_{ijk}^{(2)} = -N\frac{e^3}{\hbar^2}\sum_{g,n,n'}\left[\frac{\langle g|r_i|n\rangle\langle n|r_j|n'\rangle\langle n'|r_k|g\rangle}{(2\omega-\omega_{ng}+i\Gamma_{ng})(\omega-\omega_{n'g}+i\Gamma_{n'g})}+\cdots\right]\rho_g^{(0)}. \tag{10}$$

This expression describes a sequence of electronic transitions; two photons with energy $\hbar\omega$ excite the system from an initial state $|g\rangle$ to intermediate states $|n'\rangle$ and $|n\rangle$. A SHG photon with energy $2\hbar\omega$ is emitted when the system relaxes back to the initial state $|g\rangle$. As already mentioned above, the process of SHG is resonantly enhanced when either the fundamental photon energy $\hbar\omega$ or SHG photon energy $2\hbar\omega$ coincides with real transitions in the medium with energies $\hbar\omega_{ng}$, $\hbar\omega_{n'g}$, or $\hbar\omega_{n'n}$. In Eq. (10) N represents a unit density, Γ_{ng} is a damping constant representing the linewidth or characteristic relaxation time for transitions between quantum states, and $\rho_g^{(0)}$ denotes the population of state $|g\rangle$.

Erley *et al.*[50] developed a theory to decompose spectroscopic SHG data into a number of separate resonant contributions. In this approach the spectroscopic SHG intensity is reproduced by[18,50]

$$I(2\omega) = |\sum_L \sum_{\alpha\beta\gamma} A_{L,\alpha\beta\gamma}(\omega,\theta)\chi_{L,\alpha\beta\gamma}^{(2)}(2\omega)|^2 I_{\text{in}}^2(\omega), \tag{11}$$

where $I_{\text{in}}(\omega)$ is the intensity of the incident fundamental radiation. The subscripts L in this equation refer to the spatial origin or location of the resonances. The factors $A_{L,\alpha\beta\gamma}(\omega,\theta)$ denote complex functions that describe the propagation of both the fundamental and the SHG radiation through the system and include linear optical phenomena such as reflection, refraction, and absorption. In Sec. II C the propagation of radiation is evaluated for a two-layer system. The second-order susceptibility is approximated by a coherent superposition of critical-point-like resonances with excitonic line shapes, such as

$$\chi_{L,\alpha\beta\gamma}^{(2)}(2\omega) \propto \sum_q \frac{h_q e^{i\varphi_q}}{2\omega-\omega_q+i\Gamma_q}, \tag{12}$$

where h_q denotes the (real) amplitude, ω_q the frequency, Γ_q the linewidth, and φ_q the excitonic phase of resonance q. The excitonic line shape represents the best approximation for the E_1 CP in the linear dielectric function ε of bulk c-Si.[9] However, this approximation has proven to be useful for other transitions as well.[5,7,8,50] For the approximation in Eq. (12), it is assumed that the SHG response is resonant at the SHG photon energy with the fundamental photon energy far from a resonance. In case the fundamental photon energy is chosen to be resonant with direct interband transitions, Eq. (12) can be applied with 2ω in the denominator replaced by ω.

In addition to the phenomenological description evaluated so far, SHG can be described by bond models that have recently been developed. These models, such as the simplified bond hyperpolarizability model (SBHM)[51] and the anisotropic bond model (ABM),[52] can relate SHG to microscopic bonds on the atomic level instead of macroscopic susceptibility components. In the SBHM the nonlinear optical response of an interface is described as dipole radiation originating from the anharmonic motion of bond charge along bond directions.[51,53,54] The ABM is a very recent generalization of the SBHM, where charge motion transverse to the bond is also included.[52] These models are promising to provide an improved microscopic understanding of SHG.

C. Propagation of radiation in multilayer systems

In systems consisting of multiple layers, the propagation of radiation is an important aspect that should be considered when applying SHG. Due to multiple reflections in the layers, interference effects can occur that affect the electric fields of both the fundamental and the SHG radiation. As a result, SHG contributions from the surface and interface can have a different impact on the observed SHG intensity. These interference effects can also cause modulations in the SHG intensity with varying film thickness or photon energy. Here the propagation effects will be evaluated in a two-layer multiple reflection model taking into account SHG generated at the surface and the buried interface of the system. Extending the approach to more layers is straightforward. Alternatively, the propagation of fundamental and second-harmonic radiation through a multilayer system can be evaluated using normal mode or transfer matrix formalisms.[55,56]

The multiple reflection model consists of a semi-infinite substrate and a film with thickness d embedded in vacuum. These layers and the vacuum are referred to as media 3, 2, and 1, respectively. The geometry is depicted schematically in Fig. 2. To evaluate the different electric fields, an approach similar to Koopmans *et al.*[47,57,58] and Mizrahi and Sipe[59] is followed. In this approach an interface region between two media that generates SHG radiation is treated as a polarized sheet placed in an infinitesimal vacuum gap between the two media. In Fig. 2 these vacuum gaps are placed at $z=0^+$ and $z=-d$. In our analysis we use the convention that the local fundamental electric field at a particular interface is also evaluated within these vacuum gaps. For convenience, also the SHG electric fields are evaluated at the surface at $\mathbf{r}=(0,0,0^+)$. Other conventions would basically result in a rescaling of the elements of the second-order nonlinear susceptibility tensor and would not affect the outcome of the analysis.

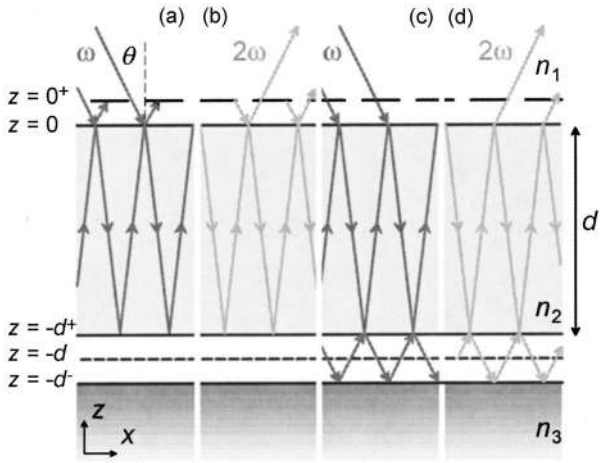

FIG. 2. Two-layer optical model to describe the propagation of fundamental and SHG radiation. The model consists of a semi-infinite substrate and a film of thickness d embedded in vacuum with refractive indices n_3, n_2, and n_1, respectively. SHG is generated in polarized sheets placed in vacuum gaps at the surface ($z=0^+$) and the buried interface ($z=-d$). Multiple reflections are displayed schematically for (a) fundamental radiation creating an electric field at the surface, (b) SHG radiation generated at the surface, (c) fundamental radiation creating an electric field at the buried interface, and (d) SHG radiation generated at the buried interface. For clarity, dispersion effects, generally occurring in the film and included in the model, are not shown.

Consider a medium i described by dielectric constant ε_i or (complex) refractive index $n_i=\sqrt{\varepsilon_i}$. The propagation direction of a beam propagating in this medium is described by the wave vector $\mathbf{k}_{i-}=k_{ix}\hat{x}-k_{iz}\hat{z}$, where k_{iz} is the positive z component defined by $k_{iz}=(\varepsilon_i k^2-k_{ix}^2)^{1/2}$, with $k=\omega/c$ the wave number in vacuum. The $-$ sign in the index of $\mathbf{k}_{i-}$ indicates that the beam has a component in the negative $\hat{z}$ direction. The propagation angle is given by $\theta_i=\arctan(k_{ix}/k_{iz})$. Reflection and transmission of radiation propagating from medium i to medium j are described by the Fresnel reflection and transmission coefficients,[57,59]

$$r_{ij}^s=\frac{k_{iz}-k_{jz}}{k_{iz}+k_{jz}},\quad r_{ij}^p=\frac{k_{iz}\varepsilon_j-k_{jz}\varepsilon_i}{k_{iz}\varepsilon_j+k_{jz}\varepsilon_i},$$

$$t_{ij}^s=\frac{2k_{iz}}{k_{iz}+k_{jz}},\quad t_{ij}^p=\frac{2k_{iz}n_in_j}{k_{iz}\varepsilon_j+k_{jz}\varepsilon_i}. \tag{13}$$

These Fresnel coefficients can be represented in a compact way by the following diagonal Fresnel transformation tensors:

$$\vec{r}_{ij}=r_{ij}^{xx}\hat{x}\hat{x}+r_{ij}^{yy}\hat{y}\hat{y}+r_{ij}^{zz}\hat{z}\hat{z}=-r_{ij}^p\hat{x}\hat{x}+r_{ij}^s\hat{y}\hat{y}+r_{ij}^p\hat{z}\hat{z},$$

$$\vec{t}_{ij}=t_{ij}^{xx}\hat{x}\hat{x}+t_{ij}^{yy}\hat{y}\hat{y}+t_{ij}^{zz}\hat{z}\hat{z}=\frac{n_ik_{jz}}{n_jk_{iz}}t_{ij}^p\hat{x}\hat{x}+t_{ij}^s\hat{y}\hat{y}+\frac{n_i}{n_j}t_{ij}^p\hat{z}\hat{z}. \tag{14}$$

The incident electric field at frequency ω propagating in vacuum (medium 1) at angle of incidence θ is given by

$$\mathbf{E}_{1-}(\omega,\mathbf{r})=\mathbf{E}_{\text{in}}(\omega,\mathbf{r})=E_{\text{in}}(\omega)e^{i\mathbf{k}_{1-}\cdot\mathbf{r}}\hat{e}_{\text{in}}, \tag{15}$$

where $\mathbf{r}=(x,y,z)$ is the position vector and $\hat{e}_{\text{in}}=\mathbf{E}_{\text{in}}/|\mathbf{E}_{\text{in}}|$ is the polarization vector or normalized incident electric field, with $\hat{e}_{\text{in}}\cdot\mathbf{k}_{1-}=0$. The local fundamental electric field at the surface at $\mathbf{r}=(0,0,0^+)$ can be related to the normalized incident field by

$$\mathbf{e}_S(\omega)=\left(\vec{1}+\vec{r}_{12}+\vec{t}_{12}\vec{r}_{23}\left(\sum_{w=0}^{\infty}[\vec{r}_{21}\vec{r}_{23}e^{2ik_{2z}d}]^w\right)\vec{t}_{21}e^{2ik_{2z}d}\right)\hat{e}_{\text{in}}, \tag{16}$$

where $\vec{1}=\hat{x}\hat{x}+\hat{y}\hat{y}+\hat{z}\hat{z}$ denotes the identity tensor. The different terms of Eq. (16) can be understood by examining Fig. 2(a). The first two terms, $\vec{1}+\vec{r}_{12}$, indicate the incident beam and the beam reflected at the surface, respectively. The other terms describes multiple reflections within medium 2. First consider a single pass through medium 2, which is denoted by $w=0$ in the summation. The radiation is transmitted from medium 1 into medium 2, as described by $\vec{t}_{12}$. The transmitted radiation reflects at the buried interface with medium 3 and, although at this interface a vacuum gap is placed, the reflection can be represented by $\vec{r}_{23}$. The use of $\vec{r}_{23}$ will be explained below. Finally, the radiation is transmitted back from medium 2 into medium 1, as described by $\vec{t}_{21}$. Due to the propagation through the film the radiation has exhibited a phase difference of $e^{2ik_{2z}d}$. Radiation exhibiting a second pass through the film ($w=1$) is, instead of being directly transmitted at the surface into medium 1, first reflected back into the film, denoted by $\vec{r}_{21}$. The second reflection at the buried interface with medium 3 and the propagation through the film result in an additional factor $\vec{r}_{23}e^{2ik_{2z}d}$. Consequently, every additional pass leads to a term with an additional factor $\vec{r}_{21}\vec{r}_{23}e^{2ik_{2z}d}$. Equation (16) can be simplified by evaluating the summation and by using the relation

$$\vec{t}_{ij}\vec{t}_{ji}=(\vec{1}+\vec{r}_{ij})(\vec{1}+\vec{r}_{ji}). \tag{17}$$

This results in

$$\mathbf{e}_S(\omega)=\frac{(\vec{1}+\vec{r}_{12})(\vec{1}+\vec{r}_{23}e^{2ik_{2z}d})}{\vec{1}-\vec{r}_{21}\vec{r}_{23}e^{2ik_{2z}d}}\hat{e}_{\text{in}}. \tag{18}$$

The reflection at the buried interface is described in Eqs. (16) and (18) by the reflection tensor $\vec{r}_{23}$. The validity of $\vec{r}_{23}$ is not influenced by the introduction of a conceptual vacuum gap at the interface. The reflection and the transmission of radiation at the interface with the conceptual gap and multiple reflections within the gap, as depicted schematically in Fig. 2(c), can be shown to reduce to $\vec{r}_{23}$,

$$\vec{r}_{21}+\vec{t}_{21}\vec{r}_{13}\sum_{v=0}^{\infty}[\vec{r}_{12}\vec{r}_{13}]^v\vec{t}_{12}=\vec{r}_{21}+\frac{\vec{t}_{21}\vec{r}_{13}\vec{t}_{12}}{\vec{1}-\vec{r}_{12}\vec{r}_{13}}=\vec{r}_{23}. \tag{19}$$

Note that k_{2z} in the factors $e^{2ik_{2z}d}$ in Eqs. (16) and (18) is generally complex. The imaginary part of k_{2z} describes absorption of radiation within medium 2.

The local electric field of the fundamental radiation at the interface at $\mathbf{r}=(0,0,-d)$ is illustrated in Fig. 2(c) and can be related to the normalized incident field by following the same approach as for the electric field at the surface,

$$\mathbf{e}_I(\omega) = \overleftrightarrow{t}_{12}\overleftrightarrow{t}_{21}(\overleftrightarrow{1} + \overleftrightarrow{r}_{13})\left(\sum_{v=0}^{\infty}[\overleftrightarrow{r}_{12}\overleftrightarrow{r}_{13}]^v\right) \times\left(\sum_{w=0}^{\infty}[\overleftrightarrow{r}_{21}\overleftrightarrow{r}_{23}e^{2ik_{2z}d}]^w\right)e^{ik_{2z}d}\hat{e}_{\text{in}}. \quad (20)$$

In this equation multiple reflections in both the vacuum gap and medium 2 have been taken into account, as represented by the two summations. Equation (20) can be simplified by using Eqs. (17) and (19), resulting in

$$\mathbf{e}_I(\omega) = \frac{(\overleftrightarrow{1} + \overleftrightarrow{r}_{12})(\overleftrightarrow{1} + \overleftrightarrow{r}_{23})e^{ik_{2z}d}}{\overleftrightarrow{1} - \overleftrightarrow{r}_{21}\overleftrightarrow{r}_{23}e^{2ik_{2z}d}}\hat{e}_{\text{in}}. \quad (21)$$

The local normalized fundamental electric fields at the surface and the interface as given by Eqs. (18) and (21), respectively, can be represented in a compact way by introducing the diagonal tensors $\overleftrightarrow{f}_S(\omega)$ and $\overleftrightarrow{f}_I(\omega)$,

$$\mathbf{e}_L(\omega) = \overleftrightarrow{f}_L\hat{e}_{\text{in}}, \quad (22)$$

where $L \in \{S,I\}$ and

$$\overleftrightarrow{f}_L = f_L^{xx}\hat{x}\hat{x} + f_L^{yy}\hat{y}\hat{y} + f_L^{zz}\hat{z}\hat{z}, \quad (23)$$

with components

$$f_S^{\xi\xi} = \frac{(1 + r_{12}^{\xi\xi})(1 + r_{23}^{\xi\xi}e^{2ik_{2z}d})}{(1 - r_{21}^{\xi\xi}r_{23}^{\xi\xi}e^{2ik_{2z}d})},$$

$$f_I^{\xi\xi} = \frac{(1 + r_{12}^{\xi\xi})(1 + r_{23}^{\xi\xi})e^{ik_{2z}d}}{(1 - r_{21}^{\xi\xi}r_{23}^{\xi\xi}e^{2ik_{2z}d})}, \quad (24)$$

where $\xi \in \{x,y,z\}$ and $r_{ij}^{\xi\xi}$ denotes the components of the Fresnel transformation tensor for reflection as defined in Eq. (14).

The SHG radiation also exhibits multiple reflections within the thin film. As can be seen from Figs. 2(b) and 2(d) the reflections encountered by SHG radiation evaluated at $\mathbf{r} = (0,0,0^+)$ are exactly the same as for the fundamental radiation. This holds for SHG radiation generated at both the surface and the buried interface. Consequently, Eqs. (23) and (24) are also valid for the SHG radiation. For clarity, the tensors describing multiple reflections of the SHG radiation will be shown in upper case. In analogy with the expression for the fundamental radiation, the propagation of the SHG electric field generated at the surface or interface and evaluated at $\mathbf{r} = (0,0,0^+)$ with polarization vector $\hat{e}_{\text{out}}$ can be represented by

$$\mathbf{e}_L(2\omega) = \hat{e}_{\text{out}} \cdot \overleftrightarrow{F}_L. \quad (25)$$

The SHG electric field from the polarized sheets projected onto the polarization vector can now be written as

$$\hat{e}_{\text{out}} \cdot \mathbf{E}_L(2\omega) = \frac{i\omega}{c\cos\theta} \times \mathbf{e}_L(2\omega) \cdot \overleftrightarrow{\chi}_L^{(2)}(2\omega):\mathbf{e}_L(\omega)\mathbf{e}_L(\omega)E_{\text{in}}^2(\omega). \quad (26)$$

For the total SHG intensity this results in

$$I(2\omega) = \frac{2\omega^2}{\varepsilon_0 c^3 \cos^2\theta} \times\left|\sum_L \mathbf{e}_L(2\omega) \cdot \overleftrightarrow{\chi}_L^{(2)}(2\omega):\mathbf{e}_L(\omega)\mathbf{e}_L(\omega)\right|^2 I_{\text{in}}^2(\omega). \quad (27)$$

This expression can be applied, for example, as a more explicit representation of Eq. (11) to reproduce spectroscopic SHG data. The SHG intensity in Eq. (27) is evaluated in vacuum, which can be replaced by an arbitrary dispersive medium i by exchanging $\cos^2\theta$ in the denominator of Eq. (27) by $n_i(2\omega)n_i^2(\omega)\cos^2\theta_i(2\omega)$.

III. EXPERIMENT

A. Laser systems

The SHG experiments that are presented in this article were mainly carried out using a femtosecond Ti:sapphire oscillator [Spectra Physics (SP) Tsunami] tunable in the 1.33–1.75 eV photon energy range (710–930 nm). This Ti:sapphire oscillator is regeneratively mode locked with an acousto-optic modulator and operates at a repetition rate of 80 MHz. For the SHG experiments the spectral width was set to 12 nm (full width at half maximum), corresponding to a pulse duration of ~90 fs. To pump the oscillator a cw $Nd:YVO_4$ laser (SP Millennia Vsj) that is intracavity frequency doubled using a lithium triborate crystal is used. The $Nd:YVO_4$ laser crystal is pumped by a fiber coupled diode bar.

Furthermore, SHG experiments were performed in the 0.76–1.14 eV photon energy range (1090–1630 nm) using the signal beam of an optical parametric amplifier (OPA) (Light Conversion TOPAS-C). This OPA is a two-stage parametric amplifier of white-light continuum. The white-light continuum is generated in a sapphire plate and overlapped noncollinearly with pump radiation in a beta-barium borate (BBO) crystal. The resulting signal beam is overlapped collinearly with pump radiation in a second BBO crystal. The OPA is pumped by a regenerative Ti:sapphire amplifier (SP Spitfire HPR). This amplifier first stretches the pulse duration of 800 nm seed pulses from the aforementioned Ti:sapphire oscillator. A selected stretched pulse is then amplified while multipassing a Ti:sapphire rod, which has been optically excited by an intracavity frequency doubled Q-switched Nd:YLF laser (SP Evolution 30). After amplification the pulse is compressed to nearly its original duration. The regenerative amplifier and the OPA operate at the repetition frequency of the diode-pumped Nd:YLF laser of 1 kHz. In this configuration the OPA radiation had a pulse duration of ~90 fs.

In addition to experiments with these femtosecond laser systems, several initial experiments were carried out using

the idler beam of an OPO pumped by a frequency tripled, injection seeded Q-switched Nd:YAG laser with a repetition rate of 30 Hz and a pulse length of 6 ns (SP MOPO 710 and GCR 230). This laser system provided radiation with a photon energy tunable between 1.05 and 1.65 eV (745–160 nm) at a linewidth of 10 cm^{-1}.[15,16]

To compare the performance of these different laser systems, it is useful to rewrite the general expression for the total SHG intensity in Eq. (27) to give the number of SHG photons $S^{2\omega}$ radiated per second,[60]

$$S^{2\omega} = \frac{\omega}{\varepsilon_0 \hbar c^3 \cos^2\theta t_p R_{\mathrm{rep}} A_s} \frac{P_{\mathrm{av}}^2(\omega)}{\times \left| \sum_L \mathbf{e}_L(2\omega) \cdot \vec{\chi}_L^{(2)}(2\omega) : \mathbf{e}_L(\omega)\mathbf{e}_L(\omega) \right|^2}. \quad (28)$$

where P_{av} is the average power in the incident beam, t_p is the pulse duration, R_{rep} is the repetition rate, and A_s is the irradiated area of the sample. Before evaluating Eq. (28) for the different laser systems, it is important to note that it is essential to keep the fluence below 100 mJ cm^{-2} to prevent damage to the c-Si.[61] This restricts the applicable range of the laser power and the beam waist. For both Ti:sapphire laser systems, the beam waist at the sample was ~ 100 μm. The applied laser power was typically 100 mW for the Ti:sapphire oscillator and 7.5 mW for the Ti:sapphire-amplifier-pumped OPA. For the Nd:YAG-pumped OPO, the beam waist was ~ 3 mm at a power of ~ 50 mW. This resulted in fluences of 16 μJ cm^{-2}, 95 mJ cm^{-2}, and 25 mJ cm^{-2} for the Ti:sapphire oscillator, Ti:sapphire-amplifier-pumped OPA, and Nd:YAG-pumped OPO, respectively. By neglecting the wavelength dependence of the SHG process, Eq. (28) results in the following ratios of the SHG photons radiated per second for the different laser systems: $S^{2\omega}_{\mathrm{Ti:S\ oscillator}} : S^{2\omega}_{\mathrm{Ti:S\ OPA}} : S^{2\omega}_{\mathrm{Nd:YAG\ OPO}} = 1 : 4\times10^2 : 10^{-2}$. Because of their ultrafast pulses, the Ti:sapphire laser systems are clearly superior to the Nd:YAG laser system in performing SHG experiments. The higher photon yield results in a better sensitivity and higher signal-to-noise ratio and the higher repetition rate results in a better time resolution.

B. Optical setup

In this section the optical setup used to generate and detect the SHG radiation is described. First the setup used in the experiments with the Ti:sapphire oscillator is treated. Subsequently, the setups for the experiments with the Ti:sapphire-amplifier-pumped OPA and the Nd:YAG-pumped OPO will be addressed.

In Fig. 3 the optical setup used in the measurements with the Ti:sapphire oscillator is displayed. The laser beam was guided to the samples using broadband silver coated mirrors (not shown). With a variable wave plate [New Focus (NF) 5540] and a Glan-Thompson polarizer (NF 5525) the desired polarization direction for the fundamental radiation was selected and the laser power at the sample was set. Any radiation at the SHG wavelength generated in the laser or in optical components in the beam path was suppressed by a

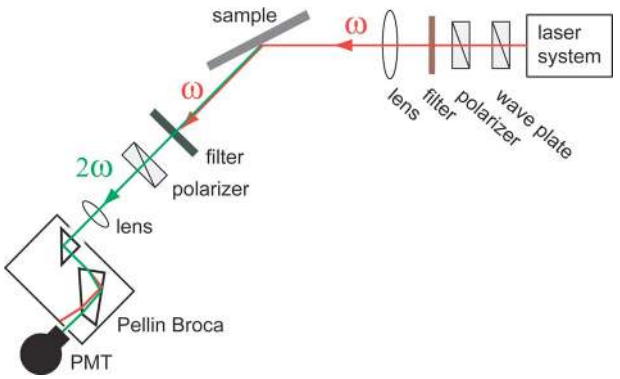

FIG. 3. Optical setup to generate and detect SHG as used in the experiments with the Ti:sapphire oscillator and the Ti:sapphire-amplifier-pumped OPA. In the experiments with the Nd:YAG-pumped OPO, a monochromator was used instead of the dispersing Pellin Broca prism.

factor of $>10^4$ using a Schott OG570 color filter. The laser beam was focused onto the sample using a plano convex BK7 lens. The polarization direction of the SHG radiation generated in reflection at the sample was selected with a Glan-Laser polarizer (Thorlabs GL10A). The fundamental radiation that reflected off the sample was suppressed by a factor $>10^6$ by two Schott BG40 color filters, blocking also possible radiation at the third-harmonic photon energy. The remaining fundamental radiation and the SHG radiation were separated spatially by a Pellin Broca dispersing prism placed between a BK7 lens and a slit. The slit blocked the remaining fundamental radiation, allowing only the SHG radiation to reach the detector. This detector consisted of a photomultiplier tube (Hamamatsu R585) connected to single photon counting electronics. The time resolution for real-time SHG experiments with this system was 0.1 s and the dark count rate of the detection scheme was below 4 Hz.

As the photon energy range in the measurements with the Ti:sapphire-amplifier-pumped OPA was different, another photomultiplier tube (Hamamatsu R928) and a different set of color filters were used in these experiments. Possible SHG radiation in the incident beam was suppressed with a Schott RG850 filter. Depending on the applied photon energy, either the combination of Schott KG3 and OG515 filters or a single Schott RG9 filter was used to suppress the fundamental radiation and any possible radiation at the third-harmonic photon energy in the outgoing beam. Furthermore, the SHG signal was beyond the applicable range of single photon counting because the number of SHG photons generated per second with this laser was typically at least two orders of magnitude larger than with the Ti:sapphire oscillator, whereas also the repetition rate was a factor of 8×10^4 lower. In this case, the charge from the photomultiplier tube was stored in a RC circuit. The discharging of the capacitor in the RC circuit was sampled with a gated 100 MHz transient recorder, providing a measure for the stored charge and, hence, the SHG intensity. The time resolution of this approach was around 2 ms. To monitor the stability of the laser system, an additional reference line was used. In this refer-

ence line, consisting of identical optical elements as the signal line, the SHG intensity from a *z* cut quartz sample with a flat spectral response was monitored.

For the experiments with the Nd:YAG-pumped OPO, photon counting was applied using the same photomultiplier tube (Hamamatsu R928) as for the Ti:sapphire-amplifier-pumped OPA experiments. The time resolution for the real-time experiments was 1 s. The filters in the incident and outgoing beams were Schott RG715 and BG39, respectively. Also for these measurements a reference channel was installed. In the initial experiments with the Nd:YAG-pumped OPO, a monochromator (Edmund NT37-598) with a resolution of 1 nm was used for the separation of the remaining fundamental and the SHG radiation. In general, the separation method using a Pellin Broca dispersing prism is more straightforward, yields less loss of SHG radiation, and is applicable over a wider photon energy range than when using a monochromator. However, combined with a charge coupled device (CCD) instead of a photomultiplier tube, a monochromator might be beneficial. For either approach, monochromator or a Pellin Broca prism, the detection bandwidth should be considered carefully when using femtosecond Ti:sapphire laser systems, which have a broad spectral width (e.g., 12 nm full width at half maximum for the oscillator).

The SHG data are represented in terms of the SHG intensity as calculated from the detected SHG signal after correction for the applied laser intensity and the response of the optical system. The optical response was obtained from separate transmission experiments of the optical components using a calibrated tungsten ribbon lamp and was verified by spectroscopic SHG experiments on single side polished *z* cut quartz. SHG experiments were carried out both *ex situ* and *in situ* using high vacuum setups. The vacuum setups were equipped with fused silica view ports to provide optical access to the samples. These viewports were verified not to generate any detectable radiation at the SHG photon energy. The second-order relation between the incident fundamental intensity and the SHG intensity was verified in the experiments.

C. Substrate and film preparation

Different thin film systems have been investigated with SHG. The common factor in all systems is the presence of silicon, either as a crystalline silicon substrate, an amorphous silicon film, or both (an amorphous silicon film on a crystalline silicon substrate).

Two types of substrates were used: Si(100) and fused silica. The Si(100) wafers (Czochralski grown, *n* type, P doped, resistivity of 10–30 Ω cm, thickness of 500 ± 25 μm) were either covered with a native oxide or terminated with hydrogen. The native oxide covered Si(100) substrates were cleaned by immersion in an ultrasound ethanol bath. The H terminated Si(100) substrates were prepared by two methods, either by ultrasound cleaning in ethanol followed by immersion in a 2% HF solution for 2 min and finally rinsing with ultrapure water or by standard RCA I and RCA II procedures using a buffered 1% NH_4F/HF solution with *p*H 4.[62] Both methods removed the native oxide terminating the Si surface with H. The fused silica substrates (thickness of 1.6 mm) were cleaned with methanol.

The thin films investigated consist of deposited *a*-Si:H, *a*-Si resulting from Ar^+-ion bombardment of *c*-Si, and aluminum oxide (Al_2O_3) prepared by plasma-assisted atomic layer deposition (ALD). The synthesis of these thin films will be addressed briefly.

The *a*-Si:H films were deposited in a high vacuum chamber (base pressure of $<10^{-9}$ mbar) from silane gas (SiH_4) by hot-wire chemical vapor deposition (HWCVD). The hot-wire source consists of a coiled 0.45 mm diameter tungsten filament that was resistively heated by a 10 A dc to a temperature of 2000 ± 200 °C. The hot wire was operated at pressures ranging from 1×10^{-4} to 8×10^{-3} mbar at a distance between 7 and 13 cm from the substrates. The substrate temperatures were typically 150 °C for experiments with Si(100) substrates and 450 °C for measurements with fused silica substrates. These conditions resulted in deposition rates ranging from 1.3 to 3.4 nm/min. Most SHG experiments on *a*-Si:H films deposited with HWCVD were performed *in situ* both during and after film deposition. The angle of incidence for these *in situ* experiments was 35°. In addition, some SHG experiments were performed *ex situ* using *a*-Si:H films deposited with radio frequency plasma enhanced chemical vapor deposition (rf PECVD) on fused silica. The deposition was carried out at 250 °C using SiH_4 as a precursor gas. The deposition pressure was 0.70 mbar and the deposition rate was 13 nm/min.

a-Si layers were formed by low-energy Ar^+-ion bombardment of H terminated Si(100). The Ar^+-ion bombardment causes damage to the surface region of the substrate, resulting in a thin layer of *a*-Si. These layers were studied *in situ* in a high vacuum chamber (base pressure of $<10^{-8}$ mbar) during and after formation of *a*-Si. The high vacuum chamber was equipped with a low-energy Ar^+-ion gun (Nonsequitur Technologies, customized version of model LEIG-2) operated on Ar gas with a purity of 99.999%. The Ar^+-ion energy ranged from 70 to 1000 eV, resulting in *a*-Si layers with a thickness on the order of a few nanometers.[18,63] The ion flux was ~0.07 ML/s (1 ML$=6.86 \times 10^{14}$ cm^{-2}). The vacuum setup also featured a XeF_2 source producing a beam of XeF_2 at a flux of ~1 ML/s. The angle of incidence of the fundamental radiation for this high vacuum system was 74°.

Ex situ SHG experiments were performed on Al_2O_3 films that were synthesized by plasma-assisted ALD at both sides of H terminated Si(100) wafers (float zone, *n* type, P doped, resistivity of 1.9 Ω cm, thickness of 275 μm). The films were deposited using $Al(CH_3)_3$ dosing alternated by O_2 plasma at a substrate temperature of 200 °C.[64] Experiments were performed with both as-grown Al_2O_3 films and with films annealed at 425 °C in N_2 for 30 min.

An important aspect in the application of SHG as a real-time surface and interface diagnostic is the possible influence of ambient species such as oxygen that might contaminate the surface. To minimize the effect of contamination in surface science studies, SHG is often performed in an ultrahigh

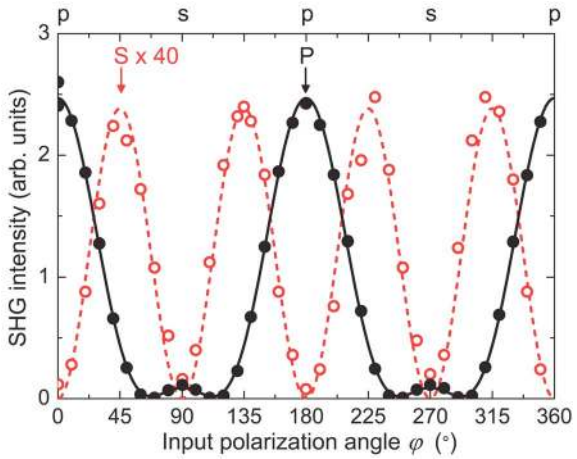

FIG. 4. Polarization dependence of the SHG intensity obtained *ex situ* from native oxide covered Si(100). Filled (open) circles represent $p(s)$ polarized SHG radiation. For clarity the s polarized SHG intensity is multiplied by a factor of 40. The polarization angle φ of the fundamental radiation is varied, where a position of 0° and 180° (90° and 270°) corresponds to $p(s)$ polarized fundamental radiation. The solid and dashed lines represent fits to the data using Eq. (4). Data were obtained using the Ti:sapphire oscillator at a SHG photon energy of 3.31 eV and an angle of incidence of 74°.

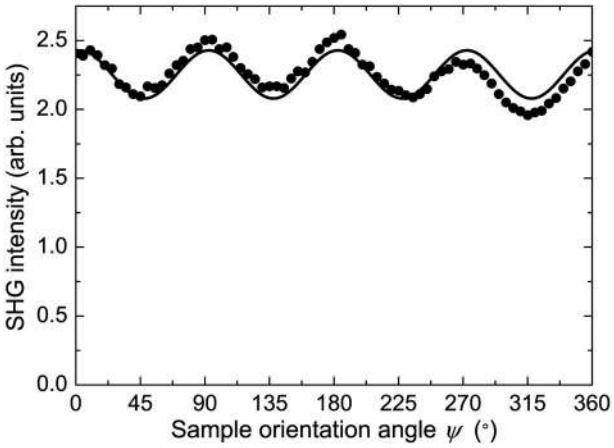

FIG. 5. Azimuthal dependence of the SHG intensity from native oxide covered Si(100) for p polarized fundamental and SHG radiation. At an orientation of 0° the plane of incidence is aligned with the [011] crystal axis. The solid lines represent fits to the data using Eq. (8). Data were obtained *ex situ* using the Ti:sapphire oscillator at a SHG photon energy of 3.31 eV and an angle of incidence of 74°.

vacuum environment ($<10^{-10}$ mbar). However, the requirements of these ultrahigh vacuum conditions can be somewhat loosened in materials processing when the flux of process-related reactive species toward the surface (e.g., ions and radicals) or the flux of volatile species away from the surface (e.g., etch products or other reaction products) is significantly larger than the flux of contaminants toward the surface. For the conditions applied during the HWCVD of a-Si:H, the radical flux toward the substrate was at least two orders of magnitude larger than the flux of possible contaminants. During the Ar^+-ion bombardment of c-Si, both the ion flux and the Si sputter rate were over an order of magnitude larger than the flux of possible contaminants toward the substrate. In *ex situ* applications of SHG, the surface will be contaminated and a native oxide might form. Nevertheless, *ex situ* experiments can yield important information on buried interfaces and on surfaces that are intended to be exposed to ambient air. In these experiments it is essential to measure under steady-state surface conditions.

IV. RESULTS OF SHG IN THIN FILM SYSTEMS

This section is basically divided into three parts. First the SHG response of the substrates applied in the different studies will be addressed. Subsequently, the "true" SHG response of films is presented by applying substrates that do not display a significant SHG response or using relatively thick films that are opaque to the SHG and/or the fundamental radiation. Finally, the SHG response of different thin film systems is described. In these cases the surface, the buried interface, and the substrate can contribute to the detected SHG intensity. Methods to separate different contributions to the SHG signal will be illustrated from the data.

A. SHG response of substrates

1. Si(100) substrates

Two types of substrates were applied in the various thin film studies: Si(100) and fused silica. The SHG response of these substrates will be discussed briefly. Figure 4 shows the polarization dependence of the SHG intensity obtained from native oxide covered Si(100). The experiments were performed using the Ti:sapphire oscillator at a SHG photon energy of 3.31 eV and an angle of incidence of 74°. Results are shown for both p and s polarized SHG radiation as a function of the polarization direction of the fundamental radiation. For p polarized SHG radiation, (local) maxima arise at purely p and s polarized pump radiation. The s polarized SHG radiation displays maxima at mixed fundamental polarization with equal s and p components. No s polarized SHG radiation is observed above the noise level for purely p or s polarized fundamental radiation. This polarization dependence corresponds to a second-order nonlinear susceptibility tensor with nonzero components $\chi^{(2)}_{zzz}$, $\chi^{(2)}_{zxx}=\chi^{(2)}_{zyy}$, and $\chi^{(2)}_{xxz}=\chi^{(2)}_{yyz}$, as expected for a Si(100) surface with $4mm$ symmetry.[32] Consequently, the polarization dependence can be reproduced well using Eq. (4) as also shown in Fig. 4. The SHG intensity clearly has a global maximum for purely p polarized fundamental and SHG radiation, which can be related to a dominant contribution of tensor component $\chi^{(2)}_{zzz}$. The importance of this component in the SHG response is enhanced by the angle of incidence of 74°, implicating relatively large electric fields in the $\hat{z}$ direction. Smaller angles of incidence would relatively increase the SHG intensity at sP and mix$S$ polarization combinations but with pP polarization remaining dominant.

In Fig. 5 the dependence of the SHG intensity on the orientation of native oxide covered Si(100) is shown for p polarized fundamental and SHG radiation at an angle of incidence of 74°. Figure 5 reveals a fourfold symmetry of

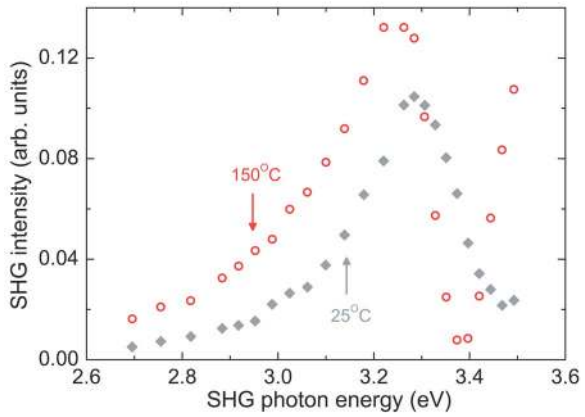

FIG. 6. SHG intensity as a function of SHG photon energy for H terminated Si(100) at room temperature and at 150 °C. Data were obtained in high vacuum at an angle of incidence of 35°. The fundamental and SHG radiation were *p* polarized with the fundamental radiation provided by the Ti:sapphire oscillator.

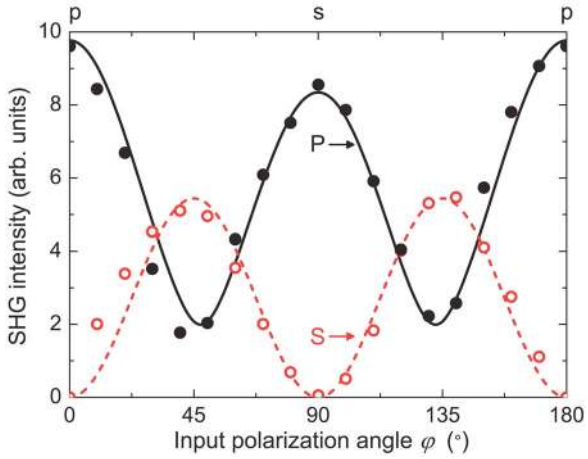

FIG. 7. Polarization dependence of the SHG intensity obtained *ex situ* from a 9 nm thick *a*-Si:H film deposited on fused silica by rf PECVD. Filled (open) circles represent *p*(*s*) polarized SHG radiation. The polarization of the fundamental radiation is varied, where a position of 0° and 180° (90°) corresponds to *p*(*s*) polarized fundamental radiation. The solid and dashed lines are fits to the data using Eq. (4). Data were obtained using the Nd:YAG-pumped OPO at a fundamental photon energy of 1.17 eV and an angle of incidence of 45°.

Si(100) upon rotation around the surface normal, in agreement with the results reported by Tom *et al.*[42] As discussed in Sec. II A, the response of the Si(100) surface is fully isotropic. The anisotropy in the signal is related to the Si(100) bulk and is described by the term proportional to ζ in Eq. (7). The azimuthal dependence of the SHG intensity in Fig. 5 can be reproduced well by fitting the expression in Eq. (8) to the data. It can be estimated that the amplitude of the anisotropic contribution is only ~5% of the total SHG electric field. In all further experiments the Si(100) substrates were oriented with the [110] crystal axis parallel to the plane of incidence of the laser beams.

For many SHG studies presented in this work, H terminated Si(100) substrates prepared by wet-chemically cleaning were used. In Fig. 6 SHG spectra for H terminated Si(100) obtained in high vacuum at room temperature and at 150 °C are shown. A sharp and asymmetric spectral feature around a SHG photon energy of 3.3 eV was obtained at room temperature, while a spectrum with a maximum at 3.25 eV and a sharp minimum at 3.4 eV was obtained at 150 °C. These SHG spectra correspond well to spectra obtained by Dadap *et al.*[4] for H terminated Si(100). As reported by Dadap *et al.*[4] the spectral features can be attributed to interfering contributions: (1) a component related to interface-modified Si–Si bonds near 3.3 eV, (2) a surface EFISH contribution near 3.4 eV, and (3) a nonresonant contribution at higher photon energies. The temperature dependence of these interfering contributions causes the difference between the spectra at room temperature and 150 °C in Fig. 6.

2. Fused silica substrates

No detectable SHG response was observed for the fused silica substrates, as expected considering the band gap of this material of 9 eV. The application of these substrates facilitates the interpretation of the SHG signal from a thin film system as the presence of substrate bulk signal can be ruled out.

B. SHG response of thin films

1. Nonresponding substrates

In Fig. 7 the polarization dependence of the SHG intensity is shown for an *a*-Si:H film with a thickness of 9 nm deposited on fused silica by rf PECVD. The experiments were performed *ex situ* using the Nd:YAG-pumped OPO system at a fundamental photon energy of 1.17 eV and an angle of incidence of 45°. Similar as for the native oxide covered Si(100), (local) maxima arise at *pP*, *sP*, and mix*S* polarizations and no SHG is observed at *pS* and *sS* polarizations. The polarization dependence can be reproduced well by Eq. (4).

In addition to the polarization dependence, the azimuthal dependence of the SHG intensity from *a*-Si:H on fused silica was measured by rotating the samples around the axis normal to the surface. Figure 8 shows the SHG signal as a function of the orientation of an *a*-Si:H film with a thickness of 4 nm deposited by rf PECVD on fused silica for the three polarization configurations corresponding to the (local) maxima of the SHG signal, *pP*, *sP*, and mix*S*. It is evident that the SHG signal does not depend on the azimuthal orientation of the sample. This indicates that the origin of the SHG signal is isotropic. As the fused silica substrates do not contribute to the SHG signal, the polarization dependence and the azimuthal dependence can be attributed to the *a*-Si:H film. The polarization and azimuthal scans correspond to a second-order nonlinear susceptibility tensor with nonzero components $\chi^{(2)}_{zzz}$, $\chi^{(2)}_{zxx}=\chi^{(2)}_{zyy}$, and $\chi^{(2)}_{xxz}=\chi^{(2)}_{yyz}$, as expected for an amorphous surface having ∞m symmetry.[15,32] No SHG signal was detected in SHG experiments performed at normal incidence of the fundamental radiation, corroborating the validity of the tensor for ∞m symmetry. At normal

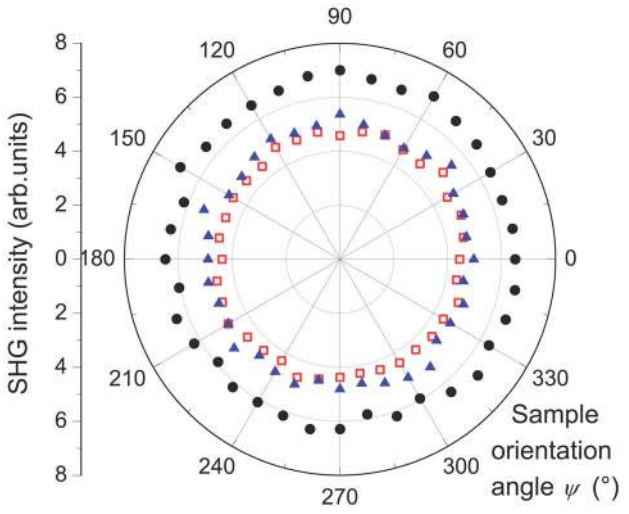

FIG. 8. Azimuthal dependence of the SHG intensity for a 4 nm thick *a*-Si:H film deposited on fused silica with rf PECVD for *pP* (filled circles), *sP* (open squares), and mix*S* (triangles) polarization configurations. Data were obtained using the Nd:YAG-pumped OPO at a fundamental photon energy of 1.17 eV and an angle of incidence of 45°.

incidence neither the fundamental nor the SHG electric fields have *z* components and consequently none of the five nonzero tensor components contribute.

In Fig. 9 the SHG spectrum for an *a*-Si:H film with a thickness of 9 nm deposited by HWCVD on fused silica is shown for *s* polarized fundamental and *p* polarized SHG radiation.[17] For the photon energy range applied, the SHG intensity increases with increasing photon energy and reflects a broad feature that, although not very clear, possibly has a maximum around a fundamental photon energy of ~1.7 eV or a SHG photon energy of ~3.4 eV. Figure 9 also shows the squared linear susceptibility $|\chi^{(1)}|^2$ of *a*-Si:H, as determined from spectroscopic ellipsometry measurements on films deposited under identical conditions.[65] Only one broad peak, centered at 3.37 eV, is observed in $|\chi^{(1)}|^2$. Following a similar argumentation as for *c*-Si,[1] the possible resemblance between the SHG spectrum and the squared linear susceptibility of the *a*-Si:H films suggests that the SHG response in the applied photon energy is governed by a two-photon resonance related to strained Si–Si bonds in the surface and/or buried interface region of the *a*-Si:H films. When compared to the spectroscopic SHG response from *c*-Si, the resonance for *a*-Si:H is much broader, which can be attributed to the disorder in the *a*-Si:H. Furthermore it is noted that the SHG spectrum resembles the spectroscopic response obtained in *in situ* experiments using the Nd:YAG-pumped OPO laser system in the fundamental photon energy range of 1.0–1.7 eV, as reported in Ref. 16.

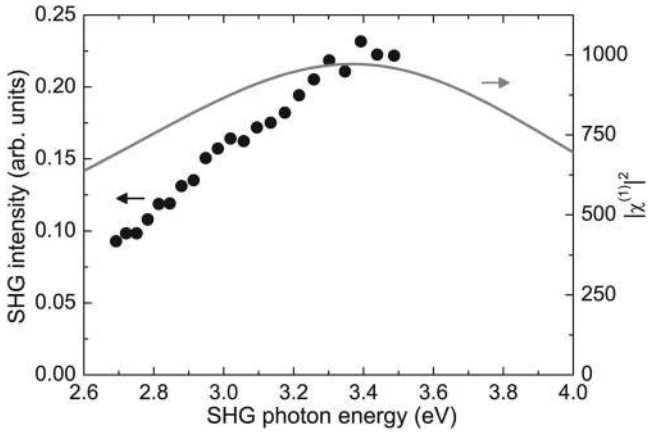

FIG. 9. SHG intensity as a function of the SHG photon energy generated at a 9 nm thick film of *a*-Si:H deposited by HWCVD on fused silica for *s* polarized fundamental and *p* polarized SHG radiation. The measurement was performed *ex situ* at an angle of incidence of 45°. The squared linear susceptibility of the *a*-Si:H as determined from spectroscopic ellipsometry measurements is also given and plotted as a function of photon energy.

2. Thick films

The use of substrates that do not generate SHG can facilitate the interpretation of the SHG response of a thin film system. However, for many applications substrates are required that inherently generate SHG. In case of films that absorb radiation, the possible SHG response from the substrate or the buried interface can be ruled out by using relatively thick films (e.g., on the order of the wavelength of the radiation) that are opaque to either both the fundamental and the SHG radiation or to solely the fundamental or the SHG radiation. For example, in the latter case the fundamental radiation can reach the interface with the substrate and possibly generate SHG radiation; however, this SHG radiation will be fully absorbed while propagating back through the film. Although the substrate and buried interface do not contribute to the SHG response for these systems, the interpretation can still be complicated because of interference effects due to multiple reflections of the fundamental radiation in the film. These effects are likely to modulate the SHG intensity generated at the surface, as discussed in Sec. II C. To illustrate the impact of interference effects, the SHG intensity was measured during deposition of an *a*-Si:H film on fused silica with HWCVD up to a thickness of ~412 nm, as shown in Fig. 10.[16] Although the fused silica substrate does not generate SHG radiation, this experiment clearly demonstrates the SHG response for thick films. The experiment was performed at *pP* polarization using the Nd:YAG-pumped OPO at a fundamental photon energy of 1.2 eV. The *a*-Si:H only slightly attenuates the fundamental radiation ($\alpha \approx 10\ \mathrm{cm}^{-1}$), whereas the SHG radiation of 2.4 eV is strongly absorbed ($\alpha = 1.3\times10^5\ \mathrm{cm}^{-1}$).[66] The SHG intensity displays a very strong dependence on the *a*-Si:H thickness, which can be explained by the propagation of the fundamental and SHG radiation through the film. Both the fundamental radiation and the SHG radiation generated at the *a*-Si:H surface and buried interface exhibit interference. However, because of the strong absorption, the influence of SHG radiation generated at the buried interface is only present at small *a*-Si:H thicknesses. In the model presented in Sec. II C this is reflected by the disappearance of $F_I^{\xi\xi}$ and, hence, $\mathbf{e}_I(2\omega)$ [Eqs. (24) and (25)] with increasing film thickness. Also multiple reflections of SHG radiation generated at the *a*-Si:H surface

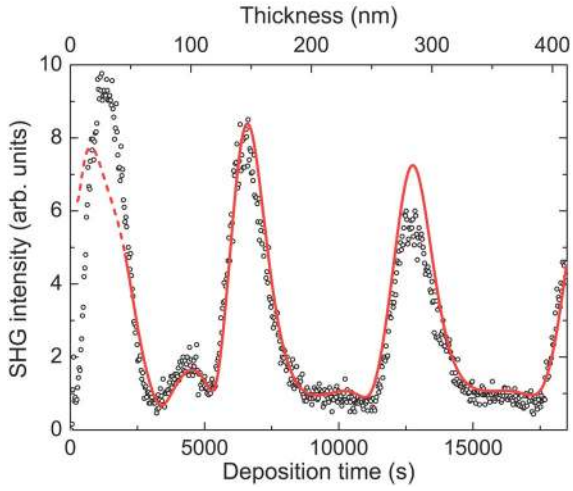

FIG. 10. SHG intensity for *pP* polarization measured during HWCVD of *a*-Si:H on fused silica. The fundamental radiation with a photon energy of 1.2 eV was provided by the Nd:YAG-pumped OPO. The solid line represents a simulation of the data using Eq. (27).

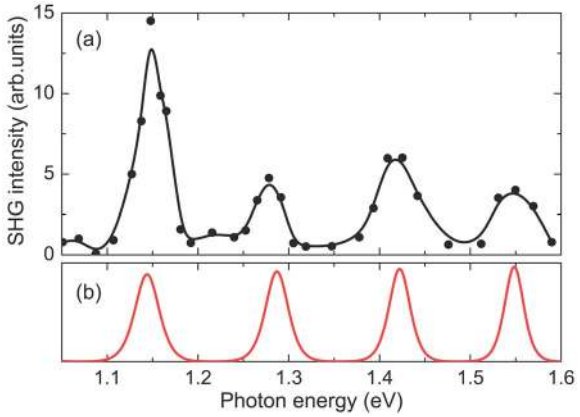

FIG. 11. (a) SHG intensity for *sP* polarization as a function of fundamental photon energy of a 1031 nm thick *a*-Si:H film deposited by rf PECVD on fused silica. Data were obtained *ex situ* using the Nd:YAG-pumped OPO at an angle of incidence of 45°. The line is a guide to the eye. (b) Simulation of the SHG spectrum of a 1031 nm thick *a*-Si:H film using Eq. (27) with the assumption that the second-order susceptibility $\vec{\chi}^{(2)}$ is photon energy independent.

contribute only to the observed SHG intensity for low *a*-Si:H thicknesses. Equivalently, $F_S^{\xi\xi}$ in Eq. (24) reduces to $1+R_{12}^{\xi\xi}$ with increasing film thickness. Therefore, the repetitive pattern of strong maxima can be assigned to interference of the fundamental radiation, resulting in a modulation of the fundamental electric field at the surface of the *a*-Si:H film. In between the strong peaks smaller features are visible that clearly decrease with film thickness. These features are caused by interference of the SHG radiation, which, while being strongly absorbed, exhibits an interference pattern with a period that is roughly a factor of 2 smaller than for the fundamental radiation.

The trend of the thickness dependence of the SHG signal can be reproduced well using Eq. (27), as given by the solid line in Fig. 10. In the evaluation we included all three tensor components $\chi_{zzz}^{(2)}$, $\chi_{zxx}^{(2)}$, and $\chi_{xxz}^{(2)}$ both at the surface and the buried interface, with $\chi_{zzz}^{(2)}$ being dominant. Both the strong peaks and the smaller features in between the strong peaks are reproduced by this description. For the first 50 nm a deviation from the experimental data occurs. This deviation is probably related to the crude assumption made for the ratio of the tensor components. Also possible changes in film structure, surface roughness, or optical properties of the film during the initial growth might be of influence.[65,67] A more detailed study including the full polarization dependence might yield more insight into the contribution of the different components. Such an approach is, for example, described by Koopmans *et al.*[47,58,68] who measured the dependence of the SHG intensity during evaporation of C_{60} films onto fused silica substrates for four different polarization configurations. This method resulted in the separation of all surface, interface, and bulk contributions to the SHG response. For this separation method, C_{60} films with a thickness on the order of the wavelength of the radiation were required.

In addition to affecting the SHG response during film growth, interference effects can also influence spectroscopic SHG data. In Fig. 11 the SHG intensity is shown for a 1031 nm thick *a*-Si:H film on fused silica as a function of the fundamental photon energy for *sP* polarization. Also in this case a strong modulation of the SHG intensity is visible. The interference pattern can be reproduced well using Eq. (27) when assuming, for simplicity, $\vec{\chi}^{(2)}$ to be independent of photon energy. Due to the *a*-Si:H film thickness of 1031 nm, any possible SHG from the substrate or buried interface is absorbed and the SHG intensity is governed solely by interference of the fundamental radiation, causing a strong modulation of the fundamental electric field at the film surface.

The two examples in this section illustrate the impact of propagation effects on the observed SHG intensity for relatively thick films. The application of these thick films provides a way to separate the surface contribution from any of the interface contributions or bulk contributions from the substrate. In the remainder of this article, we will mainly focus on thin films (<35 nm). For thin films interference and propagation effects also have a strong influence on the SHG response. However, the influence of these effects is usually not directly clear from the SHG data for thin films.

C. SHG response of thin film–substrate systems

As discussed in Sec. II A, the influence of surface, buried interface, and bulk contributions to the SHG response of a thin film system can be investigated by (1) varying the polarization of the radiation and the orientation of the sample, (2) using substrates without SHG response, (3) measuring the dependence of the SHG signal on film thickness, (4) selectively modifying surface properties, and (5) obtaining spectroscopic information. The polarization and orientation dependences of the SHG signal and the SHG response of films deposited on substrates that do not generate SHG were discussed in Sec. IV B. In the remainder of this section, strat-

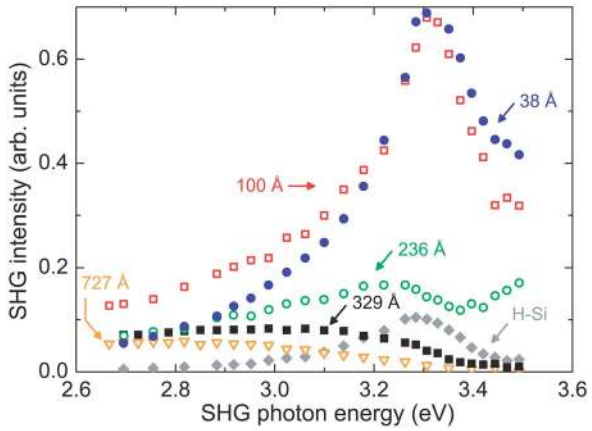

FIG. 12. SHG spectra for H terminated Si(100) and for *a*-Si:H films with a thickness ranging from 38 to 727 Å deposited by HWCVD on H terminated Si(100). Data were obtained *in situ* and at room temperature. The fundamental radiation was provided by the Ti:sapphire oscillator. Both the fundamental and SHG radiation were *p* polarized.

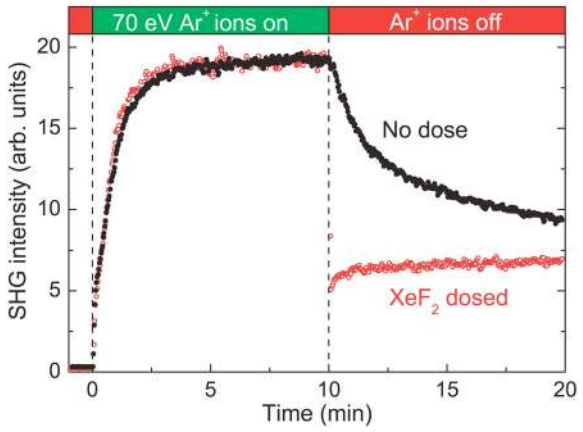

FIG. 13. SHG intensity for two H-Si(100) samples before, during, and after 70 eV Ar^+-ion bombardment. When the ion bombardment is terminated, one of the samples is dosed with ~10 ML XeF_2 (open symbols), while the other sample is not modified deliberately (solid symbols). Data were obtained at *pP* polarization with the fundamental radiation of 1.0 eV provided by the Ti:sapphire-amplifier-pumped OPA.

egies (3)–(5) will be illustrated for different thin film systems. These films have a thickness far below the wavelength of the radiation.

1. Film thickness dependence

Measuring the SHG intensity as a function of film thickness is a useful approach to gain insight into the macroscopic origin of the SHG response. *a*-Si:H films with a thickness ranging from 38 to 727 Å were deposited on H terminated Si(100) with HWCVD. The SHG experiments were performed at room temperature using the Ti:sapphire oscillator to provide the fundamental radiation. In Fig. 12 the SHG spectra obtained for the different films are shown. Also the SHG spectrum for the pristine H terminated Si(100) substrate is displayed.[20]

The SHG intensity is enhanced compared to the initial situation for ultrathin *a*-Si:H films of 38 and 100 Å. For these films a sharp resonance at ~3.3 eV is observed, similar to the H terminated Si(100) substrate. Especially the 38 Å thick film has a somewhat asymmetric appearance, indicating the presence of another contribution in addition to the strong resonance at ~3.3 eV. The presence of this additional contribution is corroborated by the spectrum for 236 Å *a*-Si:H. This spectrum shows a minimum around 3.4 eV, which is a clear indication for the presence of interfering contributions. With increasing *a*-Si:H film thickness it is evident that the SHG intensity strongly decreases, especially for high photon energies.

As discussed in Sec. II A, the Si(100) bulk can contribute to the SHG signal via the anisotropic contribution and the magnetic dipole contribution. However, the increase in SHG intensity for ultrathin films indicates that a possible substrate bulk contribution to the SHG signal is limited compared to contributions related to the *a*-Si:H. Since the SHG radiation is effectively absorbed by the *a*-Si:H, particularly at high photon energies, the decreasing trend in SHG intensity observed for increasing film thickness indicates that the SHG response is predominantly generated at the buried *a*-Si:H/*c*-Si interface. Equivalently, it can be concluded that SHG from the *a*-Si:H bulk and surface does not significantly contribute to the SHG response. Also the spectroscopic features can provide information on the macroscopic origin. The sharp resonance at ~3.3 eV observed for the 38 and 100 Å thick films is very similar to the E_0'/E_1 resonance observed for the linear susceptibility of *c*-Si.[1,9,18–20] This similarity also indicates a dominant interface contribution; the SHG signal is likely to be related to Si–Si bonds in the *c*-Si interface region. The possible additional contribution, whose presence is evident from the spectra for the 38 and 236 Å *a*-Si:H films, might be related to Si–Si bonds in the *a*-Si:H, which are expected to result in a broad contribution (see Fig. 9).[16–18]

2. Selectively modifying surface properties

To illustrate the suitability of surface modification to reveal the origin of the SHG response, two thin *a*-Si layers were prepared by 70 eV Ar^+-ion bombardment of H terminated Si(100). The 70 eV Ar^+-ion bombardment resulted in amorphized layers with a thickness of 1.8 nm.[18,63] The SHG experiments were performed with the Ti:sapphire-amplifier-pumped OPA at a fundamental photon energy of 1.0 eV. At this photon energy the SHG signal possibly originates from Si dangling bonds at the *a*-Si surface and the *a*-Si/*c*-Si interface region.[3,15,16] In addition, also the tail of the two-photon E_0'/E_1 CP resonance centered at the SHG photon energy of 3.3–3.4 eV might be of influence.[61] The two samples were bombarded for 10 min. Directly after bombardment one of the *a*-Si layers was exposed to a small dose (~10 ML) of XeF_2, terminating the surface with fluorine. The SHG intensity from both samples was measured in real time before, during, and after ion bombardment. As shown in Fig. 13, the SHG intensity increases by almost two orders of magnitude upon ion bombardment, reflecting an increase in dangling

bond density. Especially the initial increase in SHG intensity is fast; within ~10 s the intensity has already reached 25% of the final steady-state level. After this rapid initial rise the SHG intensity continues to increase but not as fast as initially. After ~4 min, steady state is reached. This behavior indicates the presence of at least two contributions to the SHG response. Because of the strong increase, the influence of substrate bulk contributions is expected to be negligible. The response to the Ar^+-ion bombardment for both samples is very similar and reflects the reproducibility of the experiment, whereas the response after terminating the ion bombardment is clearly different for both samples. For the XeF_2-dosed sample a very sharp decrease in SHG intensity is observed; within <4 s the SHG intensity has decreased to ~25% of the steady-state level during Ar^+-ion bombardment. Subsequently, the SHG intensity slightly increases again. The unexposed *a*-Si layer also displays a decreasing SHG intensity. This decrease is, however, much slower than for the XeF_2-dosed layer. Approximately 60 min after terminating the Ar^+-ion bombardment (not shown) the SHG intensity reaches the same steady-state level as for the XeF_2-dosed layer.

The XeF_2 dosing only modifies the surface of the *a*-Si layer, especially at the short time scales observed, and proves that the surface contributes to the SHG signal. A possible explanation is that surface dangling bonds created by the Ar^+-ion bombardment that contribute to the detected SHG intensity during Ar^+-ion bombardment are quenched by the XeF_2 dosing. The remaining SHG intensity after XeF_2 dosing might possibly result from dangling bonds at the *a*-Si/*c*-Si interface that is generated by the ion bombardment. The decrease displayed by the unexposed *a*-Si layer is likely related to quenching of surface dangling bonds by background species in the vacuum system. It should be noted that from the data presented here, a possible contribution from the *a*-Si bulk cannot be ruled out. A more comprehensive study including ion energy and ion flux dependent measurements will provide more insight into the origin of the SHG response and the dangling bond dynamics during Ar^+-ion bombardment of *c*-Si.[69]

Surface modification can also provide valuable information when combined with spectroscopic SHG measurements. Figure 14 shows SHG spectra for H terminated Si(100) prior to Ar^+-ion bombardment, during bombardment with 1000 eV Ar^+ ions, and after bombardment with 1000 eV Ar^+ ions and subsequent XeF_2 surface modification.[18] The spectra were obtained in the 2.7–3.5 eV SHG photon energy range using the Ti:sapphire oscillator. Also in this photon energy range the SHG intensity increases strongly due to the ion bombardment, again indicating limited influence of the substrate bulk on the SHG intensity. XeF_2 dosing of the *a*-Si surface clearly results in a different SHG spectrum with a more symmetric spectral feature compared to the spectrum obtained during ion bombardment. This clear difference shows that also in the 2.7–3.5 eV SHG photon energy, the *a*-Si surface is likely to contribute to the SHG response. More information on the microscopic origin of this surface contribution as well as the possible influence of other contributions, e.g., from the buried interface, can be obtained by considering the spectroscopic information in more detail. This will be shown in Sec. IV C 3, where the SHG spectra obtained during Ar^+-ion bombardment and after XeF_2 dosing are deconvoluted using the excitonic model discussed in Sec. II B.

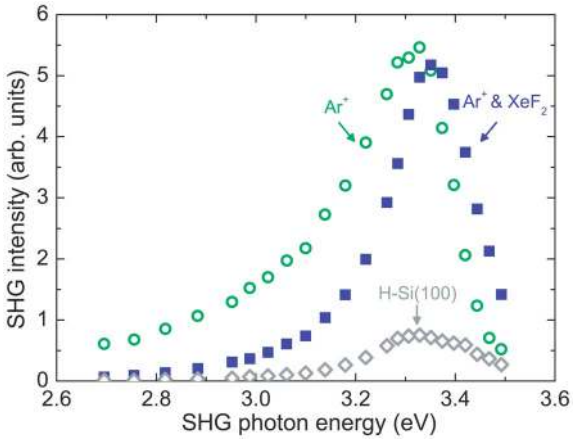

FIG. 14. SHG intensity as a function of the SHG photon energy for H terminated Si(100) prior to Ar^+-ion bombardment (open diamonds), during bombardment with 1000 eV Ar^+ ions (open circles), and after subsequent ~400 ML XeF_2 dosing (closed squares). Data were obtained *in situ* at *pP* polarization with the fundamental radiation provided by the Ti:sapphire oscillator.

3. Spectroscopic information

Spectroscopic data inherently reflect the microscopic origin of the SHG response of a material. In addition, spectroscopic data might also yield important information on the macroscopic origin of the SHG response as certain resonances can only be ascribed to specific regions in a thin film system. For example, the symmetric spectral feature in Fig. 14 measured after XeF_2 dosing shows good resemblance with the *c*-Si E_0'/E_1 CP resonance in the linear susceptibility. This indicates that the SHG response has a similar microscopic origin and likely originates from the *c*-Si interface region. Consequently, the SHG signal obtained during ion bombardment of *c*-Si is likely to have contributions from both the *a*-Si/*c*-Si interface region and the *a*-Si surface. This information is an important starting point to deconvolute the SHG spectra obtained during Ar^+-ion bombardment and after XeF_2 dosing. The spectra can be reproduced by applying the critical point model given by Eqs. (11) and (12) using two resonances, one at the buried interface ($L=I$) and one at the *a*-Si surface ($L=S$). The amplitudes h_q, frequencies ω_q, linewidths Γ_q, and phase difference φ_q are fitting parameters. The propagation of the fundamental and SHG radiation through the *a*-Si thin layer is taken into account by applying Eq. (27), where the linear optical properties of the *a*-Si and *c*-Si were obtained from spectroscopic ellipsometry.[18] The spectra have been analyzed in terms of tensor element $\chi^{(2)}_{zzz}$, as the influence of elements $\chi^{(2)}_{zxx}$ and $\chi^{(2)}_{xxz}$ is expected to be minor. This simplification as well as the exact fitting procedure is explained in Ref. 18. In Fig. 15 the fits to the SHG

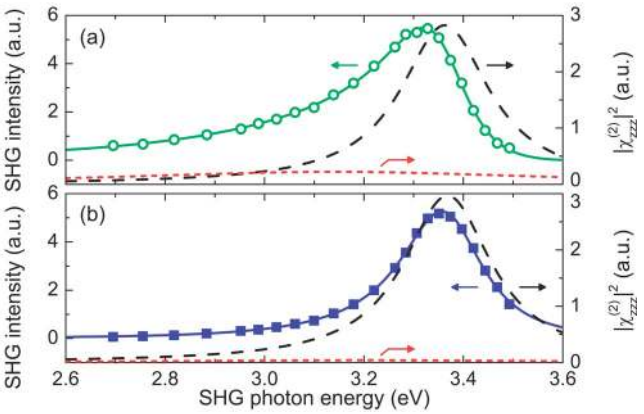

FIG. 15. Experimental (symbols) and simulated (solid lines) SHG spectra for H terminated Si(100) (a) during bombardment with 1000 eV Ar^+ ions and (b) after XeF_2 dosing immediately following 1000 eV Ar^+-ion bombardment. The dashed and dotted lines represent the individual resonances at the buried interface and the surface, respectively.

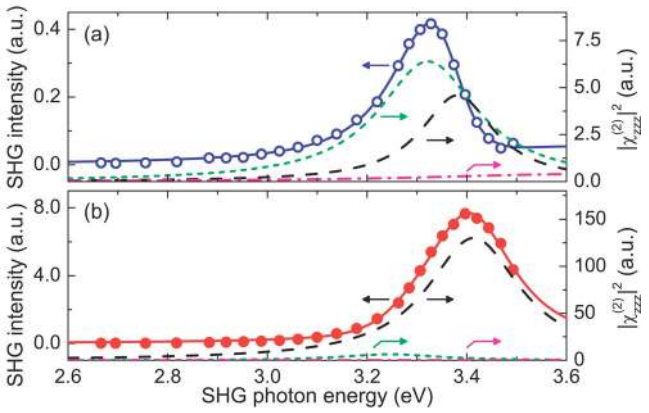

FIG. 16. SHG spectra for an 11 nm Al_2O_3 film on Si(100), (a) as-deposited and (b) after anneal. The solid lines are fits to the data using a superposition of three CP-like resonances. The dotted, dashed, and dot-dashed lines represent the individual resonances at the buried interface between *c*-Si and Al_2O_3. Data were obtained *ex situ* at an angle of incidence of 35° at *pP* polarization with the fundamental radiation provided by the Ti:sapphire oscillator.

spectra during 1000 eV Ar^+-ion bombardment and after XeF_2 dosing are shown together with the individual resonances at the surface and interface. The fits reproduce both spectra well and confirm the presence of SHG contributions at the surface and interface of the *a*-Si. For both spectra a sharp interface contribution at 3.36 eV with a linewidth of 0.1 eV is found. This contribution from the *a*-Si/*c*-Si interface does not change with XeF_2 dosing and corresponds, as expected, very well with the E_0'/E_1 CP resonance of *c*-Si, indicating that it is related to Si–Si bonds in the *c*-Si modified due to the vicinity of the interface with the *a*-Si. The surface contribution at about 3.16 eV is much weaker and is, with a linewidth of ~0.5 eV, also much broader. In the spectrum obtained after XeF_2 dosing, this contribution has almost completely disappeared and the sharp *c*-Si-like contribution from the buried interface is clearly dominant. The surface contribution shows reasonable resemblance with the spectrum for *a*-Si:H deposited on fused silica by HWCVD shown in Fig. 9, which also displays a broad feature. From the sharp *c*-Si-like feature remaining after XeF_2 dosing, it can, in addition, be concluded that contributions from the *a*-Si bulk have no significant influence, as any *a*-Si bulk contribution would most likely also result in a broad spectral feature. More information on the possible microscopic origin of the contributions as well as on the fitting parameters can be found in Ref. 18.

Another example illustrating the merits of spectroscopic experiments to reveal the origin of SHG signals is given in Fig. 16. SHG spectra were obtained from an 11 nm thick amorphous Al_2O_3 film deposited with plasma-assisted ALD on H terminated Si(100). Between the Al_2O_3 and the Si(100) an ~1.5 nm thick interfacial oxide (SiO_x) was present. Figure 16(a) shows the SHG spectrum for the as-grown film and in Fig. 16(b) the SHG spectrum is shown after an anneal at 425 °C in N_2 for 30 min.[21] The spectra were obtained in the 2.7–3.5 eV SHG photon energy range using the Ti:sapphire oscillator. Prior to anneal, a somewhat asymmetric spectral feature with a maximum at ~3.3 eV is obtained. The anneal has a strong effect on the SHG spectrum; the amplitude increases with more than an order of magnitude, whereas the peak blueshifts to ~3.4 eV, resulting in a more symmetric feature. Similar for the spectra for HWCVD *a*-Si:H on Si(100) and for *a*-Si created by Ar^+-ion bombardment of Si(100), the sharp resonances in the 3.3–3.4 eV SHG photon energy range indicate that the spectra for Al_2O_3 on Si(100) are dominated by contributions related to the *c*-Si E_0'/E_1 CP.

The spectra for the Al_2O_3 thin film have been deconvoluted using the CP model given by Eq. (12), with propagation effects taken into account by applying Eq. (27). The spectra could be reproduced well with three resonances. These contributions were all assumed to originate from the buried oxide/*c*-Si interface because of the *c*-Si-like appearance of the spectral features. Furthermore, considering the high band gap of 6.8 eV for ALD-grown amorphous Al_2O_3, a contribution from the Al_2O_3 is not likely.[70] The spectrum for the as-grown Al_2O_3 film was reproduced with (1) a dominant contribution at 3.32 eV, (2) a contribution at 3.38 eV, and (3) a broader minor contribution at 3.62 eV. The simulated spectrum for the as-grown Al_2O_3 film and the three separate resonances are also displayed in Fig. 16(a). As shown in Fig. 16(b), the spectrum after anneal could be reproduced with (1) a redshifted contribution at 3.25 eV, (2) a clearly dominant contribution at a slightly blueshifted central energy of 3.41 eV with an amplitude that increased by a factor of 6 compared to the situation prior to anneal, and (3) a contribution at 3.62 eV, which remained unmodified from the as-deposited film. The fitting procedure used to reproduce the spectra is explained in more detail in Ref. 21.

Similar for the *a*-Si films the deconvolution of the spectra indicates that the buried film/substrate interface is most likely the source of the SHG response. The contribution at ~3.3 eV is likely to originate from Si–Si bonds in the *c*-Si modified due to the vicinity of the interface with the Al_2O_3 film. The minor contribution at 3.62 eV might be related to

Si bonds in a thin transition layer between *c*-Si and the oxide.[5,7,21] The contribution around 3.4 eV is a clear indication of EFISH and the presence of a Si space-charge region. The Si space-charge region is predominantly caused by charge trapped in the Al_2O_3. A phase difference of $\sim\pi$ was found between the contribution at ~3.3 eV and the EFISH contribution, indicating a positively charged Si space-charge region and, hence, a negative fixed charge in the Al_2O_3. The strong increase in the amplitude of this contribution indicates that the negative fixed charge density in the Al_2O_3 increases due to the anneal. In Ref. 21 an approach is discussed to quantify the negative fixed charge density in the Al_2O_3.

It is interesting to note that the SHG spectra for the different kinds of thin films (*a*-Si:H, *a*-Si, and Al_2O_3) on Si(100) presented in this section display unambiguous similarities. For all these systems, with films not thicker than the escape depth of the SHG radiation, the SHG response in the 2.7–3.5 eV SHG photon energy range is governed by sharp contributions originating from the buried interface with the Si(100). For (hydrogenated) amorphous Si films these *c*-Si-like contributions interfere with broad film-related resonances, whereas Al_2O_3 films influence the *c*-Si interface SHG response by the presence of a negative fixed charge that induces EFISH.

V. CONCLUSIONS

The all-optical surface and interface sensitive technique of SHG can provide very important information on surface and interface properties during materials processing. To utilize the full potential of SHG during materials processing, insight into the origin of the SHG response is required and, particularly in thin film or multilayer systems, the propagation of radiation should be considered carefully. In this article methods have been addressed that can reveal the possible influence of surface, interface, and bulk contributions to the SHG response of thin film systems. The different methods have been illustrated by examples of SHG experiments with thin film systems relevant for Si technology, in particular, with respect to etching and deposition processes. In all the thin film systems discussed, the separation methods reveal contributions from the buried film/substrate interface with additional contributions from the film surface and indicate that the influence of bulk contributions from the substrates and the films is minor. The next steps that can provide more insight into the origin of the SHG response of thin films systems are the direct characterization of the phase of the SHG radiation and the quantification of the SHG response. The phase of the SHG response of a sample can be obtained by combining the SHG radiation with the SHG radiation from a reference sample and collecting the spectral interference pattern with a CCD.[43,71–73] Quantification can be carried out by replacing the sample in a phase measurement by a sample with well characterized nonlinear susceptibilities such as *z* cut quartz.[43,74] Detailed knowledge on the macroscopic and microscopic origins of the SHG response of thin film systems opens the path to the application of SHG during thin film processing.

ACKNOWLEDGMENTS

The authors thank M. J. F. van de Sande, J. F. C. Jansen, J. J. A. Zeebregts, and H. M. M. de Jong for their skillful technical assistance. R. F. Rumphorst is acknowledged for the design of the electronics in the SHG detection setup. This work was supported by the Netherlands Foundation for Fundamental Research on Matter (FOM).

[1] W. Daum, H.-J. Krause, U. Reichel, and H. Ibach, Phys. Rev. Lett. **71**, 1234 (1993).
[2] K. Pedersen and P. Morgen, Phys. Rev. B **52**, R2277 (1995); **53**, 9544 (1996).
[3] U. Höfer, Appl. Phys. A: Mater. Sci. Process. **63**, 533 (1996).
[4] J. I. Dadap, Z. Xu, X. F. Hu, M. C. Downer, N. M. Russell, J. G. Ekerdt, and O. A. Aktsipetrov, Phys. Rev. B **56**, 13367 (1997).
[5] G. Erley and W. Daum, Phys. Rev. B **58**, R1734 (1998).
[6] T. Suzuki, Phys. Rev. B **61**, R5117 (2000).
[7] A. Rumpel, B. Manschwetus, G. Lilienkamp, H. Schmidt, and W. Daum, Phys. Rev. B **74**, 081303(R) (2006).
[8] W. Daum, Appl. Phys. A: Mater. Sci. Process. **87**, 451 (2007).
[9] P. Lautenschlager, M. Garriga, L. Viña, and M. Cardona, Phys. Rev. B **36**, 4821 (1987).
[10] G. Lüpke, Surf. Sci. Rep. **35**, 75 (1999).
[11] J. G. Mihaychuk, J. Bloch, Y. Liu, and H. M. van Driel, Opt. Lett. **20**, 2063 (1995).
[12] J. Bloch, J. G. Mihaychuk, and H. M. van Driel, Phys. Rev. Lett. **77**, 920 (1996).
[13] Z. Marka, R. Pasternak, S. N. Rashkeev, Y. Jiang, S. T. Pantelides, N. H. Tolk, P. K. Roy, and J. Kozub, Phys. Rev. B **67**, 045302 (2003).
[14] S. Alexandrova, P. Danesh, and I. A. Maslyanitsyn, Phys. Rev. B **61**, 11136 (2000).
[15] W. M. M. Kessels, J. J. H. Gielis, I. M. P. Aarts, C. M. Leewis, and M. C. M. van de Sanden, Appl. Phys. Lett. **85**, 4049 (2004).
[16] I. M. P. Aarts, J. J. H. Gielis, M. C. M. van de Sanden, and W. M. M. Kessels, Phys. Rev. B **73**, 045327 (2006).
[17] J. J. H. Gielis, A. A. E. Stevens, P. M. Gevers, H. C. W. Beijerinck, M. C. M. van de Sanden, and W. M. M. Kessels, Phys. Status Solidi C **2**, 3968 (2005).
[18] J. J. H. Gielis, P. M. Gevers, A. A. E. Stevens, H. C. W. Beijerinck, M. C. M. van de Sanden, and W. M. M. Kessels, Phys. Rev. B **74**, 165311 (2006).
[19] J. J. H. Gielis, P. J. van den Oever, M. C. M. van de Sanden, and W. M. M. Kessels, Appl. Phys. Lett. **90**, 202108 (2007).
[20] J. J. H. Gielis, P. J. van den Oever, B. Hoex, M. C. M. van de Sanden, and W. M. M. Kessels, Phys. Rev. B **77**, 205329 (2008).
[21] J. J. H. Gielis, B. Hoex, M. C. M. van de Sanden, and W. M. M. Kessels, J. Appl. Phys. **104**, 073701 (2008).
[22] Y. D. Glinka *et al.*, Phys. Rev. B **65**, 193103 (2002).
[23] V. Fomenko, E. P. Gusev, and E. Borguet, J. Appl. Phys. **97**, 083711 (2005).
[24] R. Carriles, J. Kwon, Y. Q. An, M. C. Downer, J. Price, and A. C. Diebold, Appl. Phys. Lett. **88**, 161120 (2006).
[25] R. Carriles *et al.*, J. Vac. Sci. Technol. B **24**, 2160 (2006).
[26] B. Hoex, S. B. S. Heil, E. Langereis, M. C. M. van de Sanden, and W. M. M. Kessels, Appl. Phys. Lett. **89**, 042112 (2006).
[27] M. J. Chen, Y. T. Shih, M. K. Wu, and F. Y. Tsai, J. Appl. Phys. **101**, 033130 (2007).
[28] J. Schmidt, A. Merkle, R. Brendel, B. Hoex, M. C. M. van de Sanden, and W. M. M. Kessels, Prog. Photovoltaics **16**, 461 (2008).
[29] X. F. Hu, Z. Xu, D. Lim, M. C. Downer, P. S. Parkinson, B. Gong, G. Hess, and J. G. Ekerdt, Appl. Phys. Lett. **71**, 1376 (1997).
[30] T. F. Heinz, M. M. T. Loy, and W. A. Thompson, J. Vac. Sci. Technol. A **3**, 1467 (1985).
[31] Y. R. Shen, *The Principles of Nonlinear Optics* (Wiley, New York, 1984).
[32] T. F. Heinz, in *Nonlinear Surface Electromagnetic Phenomena*, edited by H. E. Ponath and G. I. Stegeman (Elsevier, Amsterdam, 1991), p. 353.
[33] O. A. Aktsipetrov, A. A. Fedyanin, E. D. Mishina, A. N. Rubtsov, C. W. van Hasselt, M. A. C. Devillers, and Th. Rasing, Phys. Rev. B **54**, 1825 (1996).

[34]Z. Xu, X. F. Hu, D. Lim, J. G. Ekerdt, and M. C. Downer, J. Vac. Sci. Technol. B **15**, 1059 (1997).
[35]W. Moench, *Semiconductor Surfaces and Interfaces* (Springer-Verlag, Berlin, 1995).
[36]W. Mönch, P. Koke, and S. Krueger, J. Vac. Sci. Technol. **19**, 313 (1981).
[37]S. M. Sze, *Physics of Semiconductor Devices* (Wiley, New York, 1981).
[38]N. Bloembergen, R. K. Chang, S. S. Jha, and H. Lee, Phys. Rev. **174**, 813 (1968).
[39]J. E. Sipe, D. J. Moss, and H. M. van Driel, Phys. Rev. B **35**, 1129 (1987).
[40]P. Guyot-Sionnest, W. Chen, and Y. R. Shen, Phys. Rev. B **33**, 8254 (1986).
[41]P. Guyot-Sionnest and Y. R. Shen, Phys. Rev. B **38**, 7985 (1988).
[42]H. W. K. Tom, T. F. Heinz, and Y. R. Shen, Phys. Rev. Lett. **51**, 1983 (1983).
[43]Y. Q. An, C. Carriles, and M. C. Downer, Phys. Rev. B **75**, 241307(R) (2007).
[44]X. Li, J. Willits, S. T. Cundiff, I. M. P. Aarts, A. A. E. Stevens, and D. S. Dessau, Appl. Phys. Lett. **89**, 0220102 (2006).
[45]L. Sun, P. Figliozzi, Y. Q. An, and M. C. Downer, Opt. Lett. **30**, 1377 (2005).
[46]P. Figliozzi *et al.*, Phys. Rev. Lett. **94**, 047401 (2005).
[47]B. Koopmans, Ph.D. thesis, Rijksuniversiteit Groningen, 1993.
[48]A. Wirth, J. Wei, J. J. H. Gielis, P. Figliozzi, J. Rafaelsen, Y. Q. An, and M. C. Downer, Phys. Status Solidi C **5**, 2662 (2008).
[49]L. Sun, Ph.D. thesis, The University of Texas at Austin, 2006.
[50]G. Erley, R. Butz, and W. Daum, Phys. Rev. B **59**, 2915 (1999).
[51]G. D. Powell, J.-F. Wang, and D. E. Aspnes, Phys. Rev. B **65**, 205320 (2002).
[52]E. J. Adles and D. E. Aspnes, Phys. Rev. B **77**, 165102 (2008).
[53]J. Kwon, M. C. Downer, and B. S. Mendoza, Phys. Rev. B **73**, 195330 (2006).
[54]J. F. McGilp, J. Phys.: Condens. Matter **19**, 016006 (2007).
[55]M. Born and E. Wolf, *Principles of Optics*, 7th ed. (Cambridge University Press, Cambridge, England, 1999).
[56]G. E. Jellison, Jr., Thin Solid Films **234**, 416 (1993).
[57]B. Koopmans, A. Anema, H. T. Jonkman, G. A. Sawatzky, and F. van de Woude, Phys. Rev. B **48**, 2759 (1993).
[58]B. Koopmans, A. M. Janner, H. A. Wierenga, Th. Rasing, G. A. Sawatzky, and F. van de Woude, Appl. Phys. A: Mater. Sci. Process. **60**, 103 (1995).
[59]V. Mizrahi and J. E. Sipe, J. Opt. Soc. Am. B **5**, 660 (1988).
[60]G. A. Reider and T. F. Heinz, in *Photonic Probes of Surfaces*, edited by P. Halevi (Elsevier, Amsterdam, 1995).
[61]J. I. Dadap, X. F. Hu, N. M. Russell, J. G. Ekerdt, J. K. Lowell, and M. C. Downer, IEEE J. Sel. Top. Quantum Electron. **1**, 1145 (1995).
[62]W. Kern and D. A. Puotinen, RCA Rev. **31**, 187 (1970).
[63]A. A. E. Stevens, W. M. M. Kessels, M. C. M. van de Sanden, and H. C. W. Beijerinck, J. Vac. Sci. Technol. A **24**, 1933 (2006).
[64]J. L. van Hemmen, S. B. S. Heil, J. H. Klootwijk, F. Roozeboom, C. J. Hodson, M. C. M. van de Sanden, and W. M. M. Kessels, J. Electrochem. Soc. **154**, G165 (2007).
[65]W. M. M. Kessels, J. P. M. Hoefnagels, E. Langereis, and M. C. M. van de Sanden, Thin Solid Films **501**, 88 (2006).
[66]I. M. P. Aarts, B. Hoex, A. H. M. Smets, R. Engeln, W. M. M. Kessels, and M. C. M. van de Sanden, Appl. Phys. Lett. **84**, 3079 (2004).
[67]Y. M. Li, I. An, H. V. Nguyen, C. R. Wronski, and R. W. Collins, Phys. Rev. Lett. **68**, 2814 (1992).
[68]B. Koopmans, A.-M. Janner, H. T. Jonkman, G. A. Sawatzky, and F. van der Woude, Phys. Rev. Lett. **71**, 3569 (1993).
[69]P. M. Gevers, J. J. H. Gielis, H. C. W. Beijerinck, M. C. M. van de Sanden, and W. M. M. Kessels (unpublished).
[70]J. Robertson, Solid-State Electron. **49**, 283 (2005).
[71]R. K. Chang, J. Ducuing, and N. Bloembergen, Phys. Rev. Lett. **15**, 6 (1965).
[72]K. J. Veenstra, A. V. Petukhov, A. P. de Boer, and Th. Rasing, Phys. Rev. B **58**, R16020 (1998).
[73]P. T. Wilson, Y. Jiang, O. A. Aktsipetrov, E. D. Mishina, and M. C. Downer, Opt. Lett. **24**, 496 (1999).
[74]K. Kemnitz, K. Bhattacharyya, J. M. Hicks, G. R. Pinto, K. B. Eisenthal, and T. F. Heinz, Chem. Phys. Lett. **131**, 285 (1986).